A Major Facilitator Superfamily Transporter Plays a Dual Role in Polar Auxin Transport and Drought Stress Tolerance in *Arabidopsis*

Remy, E.[a], Cabrito, T.R.[b], Baster, P.[c], Batista, R.A.[a], Teixeira, M.C.[b], Friml, J.[c,d], Sá-Correia, I.[b], and Duque, P.[a,1]

[a] Instituto Gulbenkian de Ciência, Rua da Quinta Grande, 6, 2780-156 Oeiras, Portugal

[b] Institute for Biotechnology and BioEngineering (IBB), Center for Biological and Chemical Engineering, Department of Bioengineering, Instituto Superior Técnico, Technical University of Lisbon, Av. Rovisco Pais, 1049-001 Lisbon, Portugal

[c] Department of Plant Systems Biology, VIB and Department of Plant Biotechnology and Bioinformatics, Ghent University, 9052 Gent, Belgium

[d] Institute of Science and Technology Austria (IST Austria), 3400 Klosterneuburg, Austria

[1] Address correspondence to duquep@igc.gulbenkian.pt

The author responsible for distribution of materials integral to the findings presented in this article in accordance with the policy described in the Instructions for Authors (www.plantcell.org) is: Paula Duque (duquep@igc.gulbenkian.pt).

Running head: **A Dual Function for an MFS transporter**

Estimated length: 19 printed pages

SYNOPSIS

Two plant isoforms of a single membrane transporter from the large Major Facilitator Superfamily possess the same transport activity but distinct tissue and subcellular distribution, thereby allowing this transporter to fulfill two very different physiological functions, in drought stress tolerance and root hormonal transport.

ABSTRACT

Many key aspects of plant development are controlled by the polarized transport of the phytohormone auxin. Cellular auxin efflux, the rate-limiting step in this process, has been shown to rely on the coordinated action of PIN and ABCB carriers. Here, we report that polar auxin transport in the *Arabidopsis thaliana* root also requires the action of a Major Facilitator Superfamily (MFS) transporter, ZIFL1. Sequencing, promoter-reporter and fluorescent protein fusion experiments indicate that the full-length ZIFL1.1 protein and a truncated splice isoform, ZIFL1.3, localize to the tonoplast of root cells and the plasma membrane of leaf stomatal guard cells, respectively. Using reverse genetics, we show that the ZIFL1.1 transporter regulates various root auxin-related processes, while the ZIFL1.3 isoform mediates drought tolerance by regulating stomatal closure. Auxin transport and immunolocalization assays demonstrate that ZIFL1.1 indirectly modulates cellular auxin efflux during shootward auxin transport at the root tip, likely by controlling plasma-membrane PIN2 abundance. Finally, heterologous expression in yeast revealed that ZIFL1.1 and ZIFL1.3 share H^+-coupled K^+ transport activity. Thus, by determining the subcellular and tissue distribution of two isoforms, alternative splicing dictates a dual function for the ZIFL1 transporter. We propose that this MFS carrier regulates stomatal movements and polar auxin transport by modulating potassium and proton fluxes in *Arabidopsis* cells.

INTRODUCTION

The phytohormone auxin, particularly its predominant endogenous form indole-3-acetic acid (IAA), plays a critical role in the spatial and temporal coordination of plant development. Auxin regulates a variety of unrelated processes, such as embryo, root and vascular patterning, postembryonic organogenesis and tropisms among others, by directing cell division and expansion (reviewed in Woodward and Bartel, 2005). The diversity of developmental responses mediated by auxin is determined by a specific cellular signal transduction mechanism involving perception by the Transport Inhibitor Response 1/Auxin Signaling F-Box (TIR1/AFB) receptor proteins and interpretation by a downstream nuclear signaling pathway that ultimately mediates transcriptional developmental reprogramming (reviewed in Paciorek and Friml, 2006). Many if not all aspects of auxin action rely on its differential distribution within plant tissues manifested by local auxin maxima and minima, also referred to as auxin gradients (reviewed in Tanaka et al., 2006), with the steady-state level of auxin within a particular cell triggering the developmental output of auxin signaling.

Along with metabolism, the asymmetric auxin distribution is mainly sustained by its intercellular transport, which, uniquely amongst plant signaling molecules, is strictly regulated in a directional fashion termed polar auxin transport. In the shoot, auxin flows in a single direction from its primary sites of synthesis, such as the apical meristem and developing leaves, down towards the root through the stem vascular tissues (Okada et al., 1991; Rashotte et al., 2003). By contrast, two distinct, antiparallel streams of auxin movement occur in the root. Shoot-derived auxin travels over the whole-root distance through the central stele downwards to the root apex, where after loading into the outer cell layers it is redirected over a short distance towards the base of the root (Mitchell and Davies, 1975; Tsurumi and Ohwaki, 1978; Rashotte et al., 2000). According to the current paradigm, the mechanistic basis for the polarized auxin cell-to-cell movement is better described by the chemiosmotic hypothesis, in which the proton gradient generated primarily by plasma membrane H^+-ATPases between the neutral cytoplasm and the acidic extracellular space drives cellular auxin uptake and efflux (Rubery and Sheldrake, 1974; Raven, 1975). This model postulates the existence of plasma membrane-localized auxin influx and efflux carriers, whose coupled asymmetrical localization between adjacent cells provides the directionality of cellular auxin flow (Goldsmith, 1977). These specific

transporters were later identified by chemical and genetic approaches using the model system *Arabidopsis thaliana* (reviewed in Vieten et al., 2007; Petrasek and Friml, 2009).

In the acidic apoplastic environment, a fraction of the weak acid IAA exists in its undissociated form, which can passively diffuse through the plasma membrane inside the cells, whereas the non-lipophilic and therefore less permeable proton-dissociated auxin fraction requires a carrier-mediated uptake system to enter the cell. Auxin influx is mediated by the amino acid permease-like Auxin Resistant 1 (AUX1) and three closely-related Like AUX1 (LAX) proteins that catalyze proton symport activities (Marchant et al., 1999; Yang et al., 2006; Swarup et al., 2008). Uncovered by the root auxin-resistant nature of the corresponding mutant, AUX1 was among the earliest polar auxin transporters identified and its localization to a specific side of some cell types has been shown to facilitate directional auxin transport, thereby influencing a wide array of tropic and phyllotactic processes (Bennett et al., 1996; Swarup et al., 2001; Kleine-Vehn et al., 2006). In the neutral cytosolic environment, IAA exists mainly in its membrane-impermeant anionic form that requires active transport to exit the cell. Hitherto, two distinct protein families whose members possess auxin-exporting activity have been associated with cellular polar auxin efflux. The best characterized auxin efflux carriers are members of the unique and plant-specific PIN-formed (PIN) protein family. PINs possess a predicted topology similar to ion-coupled members of the Major Facilitator Superfamily (MFS) and are believed to be secondary transporters that use proton gradients as an energy source (Petrasek et al., 2006; Wisniewska et al., 2006). By contrast, some plant homologs of the human Multidrug resistance/P-glycoprotein (MDR/PGP) transporters belonging to the B-family of ATP-binding cassette (ABC) superfamily, such as ABCB1, ABCB4 and ABCB19, have been implicated in ATP-energized auxin efflux (Geisler et al., 2005; Lin and Wang, 2005; Santelia et al., 2005; Terasaka et al., 2005). Although a few cases of asymmetric subcellular localization have been reported for ABCBs (Blakeslee et al., 2007), the bias and rate of auxin transport are mainly attributable to the highly regulated polar localization of PIN transporters (Petrasek et al., 2006; Wisniewska et al., 2006).

Based on the different, sometimes opposite, phenotypes that their auxin export activities mediate, PINs and ABCBs have been shown to define two distinct auxin efflux systems. Whereas PIN-mediated auxin efflux activity is required for polar embryogenesis, organogenesis and patterning (Reinhardt et al., 2003; Blilou et al., 2005; Weijers et al.,

2005), ABCBs contribute mainly to the export of auxin in vegetative tissues, directing long-distance auxin transport in mature plants (Lin and Wang, 2005; Wu et al., 2007). On the other hand, a concerted action of PINs and ABCBs has been highlighted in a number of recent studies demonstrating a role for ABCBs in providing IAA to the PIN proteins for vectorial transport (Mravec et al., 2008) or in stabilizing PINs at the plasma membrane in order to enhance specificity for auxin (Blakeslee et al., 2007; Titapiwatanakun et al., 2009). Therefore, both efflux transport systems may act coordinately to generate and maintain the differential distribution of auxin.

The two widest families of transporters occurring in the plant kingdom and the only known to be ubiquitous to all classes of organisms, the ABC superfamily and the MFS, share the common feature of a particularly diverse range of substrates (reviewed in Pao et al., 1998; Rea, 2007). While numerous plant ABC transporters are known to participate in such disparate processes as polar auxin transport, xenobiotic sequestration, disease resistance or stomatal regulation among others, the functional significance of the vast majority of MFS transporters in such fundamental physiological processes remains unknown. MFS transporters are single-polypeptide secondary carriers capable only of transporting small solutes in response to chemiosmotic ion gradients. According to the current annotation, the *Arabidopsis* genome contains more than 120 genes predicted to encode members of the MFS transporter family (TransportDB, www.membranetransport.org, Ren et al., 2004); TAIR10, www.arabidopsis.org, Huala et al., 2001), which have been traditionally classified according to the extensive sequence similarities they share with MFS transporters characterized in other organisms (Pao et al., 1998). To date, the few plant MFS transporters characterized have been essentially implicated in sugar, oligopeptide and nitrate transport (Buttner, 2007; Tsay et al., 2007). In addition, an *Arabidopsis* MFS member, Zinc-Induced Facilitator 1 (ZIF1), has been described as a tonoplast-localized transporter involved in zinc tolerance (Haydon and Cobbett, 2007), indicating that MFS transporters might also influence ion homeostasis in plants. We have recently shown that heterologous expression of a ZIF1 paralog, ZIF-Like 1 (ZIFL1), in *Saccharomyces cerevisiae* confers resistance to the synthetic auxin 2,4-dichlorophenoxyacetic acid (2,4-D) by reducing its concentration inside the yeast cell (Cabrito et al., 2009). Owing mainly to its high stability, 2,4-D has been used for decades

as an exogenous source of auxin in physiological studies and mutant screens, thus allowing the discovery of polar auxin transport system components (Bennett et al., 1996).

In this study, we investigated the *in vivo* roles of the *Arabidopsis* ZIFL1 transporter using a combination of functional analyses in *A. thaliana* and heterologous expression in *S. cerevisiae*. Our results reveal a previously unrecognized role for MFS transporters in modulating polar auxin transport and drought stress tolerance. This dual function is determined by alternative splicing of the *ZIFL1* gene, which allows the encoded transporter to regulate both root shootward auxin transport, by indirectly affecting cellular auxin efflux, and leaf stomatal movements.

RESULTS

The *ZIFL1* Promoter Is Predominantly Active In Root Tissues and Stomatal Guard Cells

To initiate the characterization of the *Arabidopsis thaliana ZIFL1* gene (At5g13750), we monitored its organ- and tissue-specific expression patterns by means of reporter gene experiments. Staining of transgenic lines stably expressing β-glucuronidase (GUS) under the control of the *ZIFL1* promoter revealed that the latter is active in most plant organs (Fig. 1A-L). In flowers, *ZIFL1* appears to be strongly and exclusively expressed in the anther stamen filaments at all stages of floral development (Fig. 1A). Interestingly, in young leaves *ZIFL1* expression was largely restricted to stomata, which exhibited a distinct GUS coloration (Fig. 1B). In fact, all green mature plant organs, such as stems, siliques and leaves, displayed exclusive staining of stomatal guard cells (Fig. 1C). In light- and dark-grown seedlings, very intense *ZIFL1* promoter activity was detected at the shoot apical meristem (Fig. 1D) as well as throughout the root system. Although homogenous GUS coloration was observed from the hypocotyl-root junction (Fig. 1E) through all along the primary root (PR) (Fig. 1F), the *ZIFL1* promoter was particularly active at the root tip (Fig. 1G). In addition, while no staining could be detected in lateral root (LR) primordia (Fig. 1H-K), *ZIFL1* was abundantly expressed in elongating LRs (Fig. 1L).

We further explored the precise localization of *ZIFL1* promoter activity in root tissues using transgenic lines expressing the green fluorescent protein (GFP) under the control of the *ZIFL1* promoter (Fig. 1M-P). In the mature portion of the PR, the GFP signal was

restricted to the cortex and to a lesser extent the epidermis (Fig. 1M). At the root tip, *ZIFL1* promoter activity was high in both the cortical and epidermal cell layers of the apical meristem and the transition zone, while absent from the quiescent center, the columella cells or the lateral root cap (Fig. 1N). A similar layer-specific pattern was observed in LRs, with *ZIFL1* expression appearing mainly restricted to the cortex at an early stage of LR elongation (Fig. 1O) and spreading also to the epidermis, particularly at the tip, in older LRs (Fig. 1P). By contrast, *ZIFL1* promoter activity in stomata was insufficient to allow detection of the GFP signal.

Taken together, these results indicate that ZIFL1 may exert a prominent role in roots, particularly at the PR and LR tips, as well as in stomatal guard cells.

The *ZIFL1* Gene Encodes Two Splice Isoforms, ZIFL1.1 and ZIFL1.3, Exhibiting Distinct Tissue and Subcellular Distribution

According to the current genome annotation (TAIR10; www.arabidopsis.org), the *Arabidopsis ZIFL1* gene contains 17 exons (Fig. 2A) and generates three distinct transcripts (Fig. 2B). The first, *ZIFL1.1* (At5g13750.1), corresponds to the full-length transcript resulting from constitutive splicing of the precursor mRNA (pre-mRNA), while the second, *ZIFL1.2* (At5g13750.2), likely arises from selection of an alternative transcription start site in the second intron. The predicted start codons of these two alternative transcripts are in frame, and hence their coding sequences are identical downstream of the *ZIFL1.2* ATG. Finally, the *ZIFL1.3* (At5g13750.3) splice variant derives from selection of an alternative 3' splice site in the fourteenth intron, with the second of two contiguous AGs being recognized (Fig. S1). The *ZIFL1.1* and *ZIFL1.3* transcripts are therefore identical, except for the absence of two nucleotides in *ZIFL1.3* that leads to the inclusion of a premature stop codon in the fifteenth exon. The *ZIFL1.1* transcript is predicted to encode the full-size transporter, displaying the typical MFS transporter signature motif that includes two transmembrane domains, each consisting of six membrane-spanning segments delimiting a central hydrophilic loop (Fig. 2C). On the other hand, the *ZIFL1.2* and *ZIFL1.3* transcripts encode putative transporters that retain the characteristic MFS structure but lack the two first N-terminal or the two last C-terminal membrane-spanning segments, respectively.

In order to verify the accuracy of these predictions and examine the tissue-specific distribution of the *ZIFL1* transcripts, we first undertook an RT-PCR approach. Given that the *ZIFL1.1* and *ZIFL1.3* transcripts differ by solely 2 nt, only primers concomitantly amplifying both transcripts could be designed, while an independent forward primer was used to detect *ZIFL1.2*. Consistent with the promoter activity profile shown in Figure 1, RT-PCR analysis revealed that *ZIFL1* is expressed throughout plant development (Fig. 2D), with the *ZIFL1* mRNAs being most abundant in young seedlings and root tissues, whereas very low transcript levels were detected in flowers and green tissues. The *ZIFL1.1/ZIFL1.3* and *ZIFL1.2* expression patterns were globally comparable, except that the *ZIFL1.1/ZIFL1.3* transcripts appeared to be markedly more abundant in senescent leaves and expression of *ZIFL1.2* was slightly more pronounced in flowers.

Intriguingly, during this analysis we were able to easily clone the full-length *ZIFL1.1* and *ZIFL1.2* transcripts using cDNA obtained from roots, but various attempts to isolate the third transcript from this particular tissue revealed unsuccessful. This prompted us to investigate further the endogenous tissue distribution of the *ZIFL1* transcripts by means of a sequencing approach. To this end, we PCR-amplified and sequenced a *ZIFL1* fragment, including the 2-nt deletion present only in the *ZIFL1.3* transcript, independently from root and leaf cDNA. As shown in Figure S1, when using the F4/R3 primer pair, which concomitantly amplifies the three transcripts, only the sequence corresponding to *ZIFL1.1*/*ZIFL1.2* could be detected in the *ZIFL1* fragment obtained from root tissues, whereas the *ZIFL1.3* transcript was also detectable, albeit at lower levels, in leaves. When using the F1/R3 primer pair, which amplifies specifically the *ZIFL1.1* and *ZIFL1.3* splice variants, we were only able to identify the *ZIFL1.1* sequence in the root-derived fragment, whereas a mixture of rather equivalent amounts of *ZIFL1.1* and *ZIFL1.3* was found in the fragment derived from leaf tissues. These sequencing results thus revealed clear tissue-specificity of the *ZIFL1* transcripts, with roots expressing exclusively *ZIFL1.1*/*ZIFL1.2*, while in leaves the *ZIFL1.3* splice variant also represents a significant fraction of the *ZIFL1* transcript pool.

To allow inference of the *in vivo* function(s) of the ZIFL1 transporter, we isolated two mutant alleles carrying T-DNA insertions in the *ZIFL1* gene. The first allele (SALK_030680) was designated *zifl1-1* in accordance to Haydon and Cobbett (2007), whereas the second was identified from the GABI-Kat collection (GABI_052H08) and

named *zifl1-2*. Sequence analysis of the genomic DNA/T-DNA junctions determined that both insertions are located in the eleventh exon of *ZIFL1* (see Fig. 2A). RT-PCR analysis of *ZIFL1* expression in *zifl1-1* and *zifl1-2* homozygous seedlings using primers annealing upstream of the insertion sites revealed transcript levels comparable to wild-type plants, but no expression was detected when primers flanking or annealing downstream of the T-DNA segments were used (Fig. 2E). This indicates that the two mutant alleles produce a truncated version of the three *ZIFL1* transcripts that lacks the sequence corresponding to the entire second transmembrane domain and are thus unlikely to encode functional membrane transporters (Shin et al., 2004). These results strongly suggest that both *zifl1-1* and *zifl1-2* are true loss-of-function mutants.

As the subcellular localization of the three alternative isoforms was expected to provide pivotal clues in the functional analysis of the *ZIFL1* gene, we next generated C-terminal yellow fluorescent protein (YFP) fusions of each isoform and independently cloned them under the control of the 35S promoter. Surprisingly, transient expression of these constructs in *Arabidopsis* protoplasts suggested that the ZIFL1.1-YFP fusion protein localizes to the tonoplast, whereas ZIFL1.3-YFP appears to be targeted to the plasma membrane (Fig. 3A-C). By contrast, no fluorescence could be detected in any of the transfection assays performed with the ZIFL1.2-YFP construct. To further verify the subcellular localization of the ZIFL1.1 and ZIFL1.3 isoforms, we generated stable transgenic *Arabidopsis zifl1* mutant lines carrying either *ZIFL1.1* or *ZIFL1.3* fused at the C-terminal end with the GFP sequence and placed under the control of the native *ZIFL1* promoter. Confocal microscopy analysis of root apices expressing ZIFL1.1-GFP again indicated tonoplast localization for ZIFL1.1 in both the cortical and epidermal cell layers (Fig. 3D-F), whereas no fluorescence could be detected with this fusion protein in stomatal guard cells. In agreement with the results from our promoter-GFP reporter gene experiments, we were also unable to visualize transgene-derived fluorescence in guard cells of plants expressing the ZIFL1.3-GFP fusion protein. Interestingly, in these transgenic plants no ZIFL1.3-GFP signal was detected in root apices, despite detailed analysis of a large number of independent transformants and consistent with the absence of *ZIFL1.3* transcript detected in wild-type root tissues (see Fig. S1). In order to unequivocally ascertain the subcellular localization of the ZIFL1.1 and ZIFL1.3 splice forms, we subsequently performed colocalization experiments in tobacco leaf epidermal cells using

specific tonoplast and plasma membrane markers (Nelson et al., 2007). As shown in Figure 3G-V, the ZIFL1.1-GFP fusion protein colocalized with the tonoplast marker, whereas the ZIFL1.3-GFP fusion protein matched the distribution of the plasma membrane marker. Collectively, these findings indicate that the full-length ZIFL1.1 and the truncated ZIFL1.3 transporters are localized at the tonoplast and the plasma membrane, respectively.

Loss of *ZIFL1* Function Causes Hypersensitivity to Drought Stress and Auxin-related Defects

To uncover the biological role(s) of the *Arabidopsis* ZIFL1 transporter, we carried out a detailed phenotypical analysis of the *zifl1-1* and *zifl1-2* mutants. Under optimal growth conditions, *zifl1* mutant adult plants appeared indistinguishable from the corresponding wild type (Col-0), as illustrated in Figure 4A (control conditions), showing also normal flowering time and fertility (data not shown). However, we consistently observed that *zifl1* mutant plants were more sensitive to lack of regular watering, as demonstrated by their faster wilting under limited water supply when compared with wild-type plants (Fig. 4A, drought stress conditions). This effect was quantified using a detached leaf assay and, as depicted in Figure 4B, both the *zifl1-1* and *zifl1-2* mutants clearly exhibited enhanced transpiration rates, losing between 40 and 50% of their fresh weight, versus only about 20% for wild-type plants, upon 3 h of water stress. Similar results were obtained when entire plants (rosette stage) were employed instead of detached leaves (Table 1), indicating that the ZIFL1 transporter is involved in the regulation of drought stress tolerance in *Arabidopsis*.

Guard cells play a key role in optimizing plant CO_2 uptake and concomitant water loss at the leaf interface by precisely controlling stomatal apertures in response to physiological and environmental stimuli (reviewed in Araújo et al., 2011). Together with the specific *ZIFL1* promoter activity we detected in guard cells (see Fig. 1C), the drought stress hypersensitivity of the *zifl1* mutants prompted us to investigate whether *ZIFL1* disruption affects stomatal movements. Indeed, microscopic measurements of stomatal apertures revealed that the stomatal pore was significantly larger in the *zifl1* mutants than in the wild type (Fig. 4C). This effect was relatively modest under light, but markedly more pronounced in the dark or upon treatment with the stress hormone abscisic acid (ABA),

two major effectors triggering stomatal closure (Mittelheuser and Van Steveninck, 1969; Thimann and Satler, 1979). Nevertheless, *zifl1* mutant stomata retain full sensitivity to both dark- and ABA-mediated stomatal closure, indicating that loss of *ZIFL1* function does not affect the corresponding signaling transduction pathways. These results indicate that the ZIFL1 transporter is required for efficient stomatal closure.

Given the high *ZIFL1* expression in root tissues (see Figs. 1, 2D and 3D) and the ZIFL1 heterologous expression results we obtained previously in yeast with the 2,4-D herbicide and the naturally-occuring auxin IAA (Cabrito et al., 2009), we next sought to evaluate the PR response of the *zifl1* mutants to exogenous application of these two auxins. Although PR growth was unaffected under control conditions, *zifl1-1* and *zifl1-2* mutant PR elongation exhibited hypersensitivity to the inhibitory effect of 2,4-D, as well as significantly enhanced sensitivity to inhibition by IAA, at least at low concentrations of the natural auxin (Fig. 5A and 5B; Table 1). To determine whether the identified phenotypes were restricted to root elongation, we also examined the effect of auxin application on hypocotyl elongation of dark-grown seedlings. Again no phenotype was observed under control conditions, but both 2,4-D and IAA inhibited hypocotyl elongation to a greater extent in *zifl1-1* and *zifl1-2* mutants than in the wild type (Fig. S2A). Remarkably, such an exacerbated sensitivity was not detected when *zifl1* mutant seedlings were challenged with other naturally-occurring (e.g. IBA – indole-3-butyric acid) or synthetic (e.g. 1-NAA – 1-naphthaleneacetic acid) auxinic compounds (Fig. S3), strongly suggesting that the ZIFL1 transporter confers resistance specifically to 2,4-D and IAA.

Deeper characterization of the root system architecture of seedlings grown under control conditions revealed that *zifl1* mutant and wild-type roots produce a similar number of total LR structures, including LR primordia and emerged LRs. However, the proportion of emerged LRs was reduced by about 25% in *zifl1* mutant seedlings, and these emerged LRs were significantly shorter than those of the wild type (Fig. 5A and 5C). This indicates that the *zifl1* mutants are not defective in LR initiation processes, but rather in LR emergence and/or post-emergence elongation. Furthermore, we quantitatively assessed root tip reorientation after gravity stimulation and found that both *zifl1-1 and zifl1-2* exhibit defective root gravitropic bending relative to wild-type seedlings ($P<0.001$, Student's *t* test; Fig. 5D). As no differences were observed in linear PR elongation, this phenotype is likely to result from an intrinsic defect in the gravitropic response. Therefore, the *zifl1* mutants

are impaired in two developmental processes typically triggered by auxin. In fact, this phytohormone provides a critical stimulatory signal during the two steps of LR development, the initiation and emergence phases (Wu et al., 2007; Swarup et al., 2008), eliciting also differential growth rates in response to tropisms, in particular to root gravitropism (Friml et al., 2002).

The striking phenotypical similarity displayed by the *zifl1-1* and *zifl1-2* mutant alleles strongly suggested that the observed defects result from loss of *ZIFL1* function. To exclude the possibility of the effect of a mutation in another gene, we transformed both mutants with a genomic fragment spanning the entire *ZIFL1* gene, which included the same promoter sequence used in the reporter gene experiments. The water loss rates of the corresponding transgenic complementation lines were similar to those of wild-type plants (Fig. 4B). In addition, *zifl1* complementation lines exhibited complete restoration of PR and hypocotyl elongation wild-type sensitivity to 2,4-D and IAA (Figs. 5B and S2A). Finally, genomic complementation of the *zifl1* mutants fully suppressed the LR formation (Fig. 5C) and gravitropic bending (Fig. 5D) defects. We have thus confirmed that disruption of the *ZIFL1* gene is responsible for the identified *zifl1* mutant phenotypes. Moreover, the fact that we observed full rescue of all phenotypes strongly suggests that the full-length *ZIFL1* promoter is comprised in the selected sequence.

ZIFL1.1 Functions in Auxin-related Processes While ZIFL1.3 Confers Drought Stress Tolerance

In light of the above results, we next wanted to examine the contribution of the three alternative ZIFL1 isoforms to the phenotypes established for the *zifl1* mutants. To address this issue, we first generated *Arabidopsis* transgenic lines independently expressing each *ZIFL1* transcript under the control of the 35S promoter in the wild-type background for phenotypical characterization.

Regarding the auxin-related phenotypes, we found that overexpression of *ZIFL1.1* confers increased resistance to the inhibitory effects of exogenously applied 2,4-D and IAA, both at the level of PR (Fig. 6A) and hypocotyl (Fig. S2B) elongation. Figure 6B shows that, although the number of total LR structures produced by the *ZIFL1.1*-overexpressing lines was not significantly different from the wild type, the ratio between LR primordia and emerged LRs was markedly unwedged to emerged LRs, whose length was

increased by almost 30% in these plants. Overexpression of *ZIFL1.1* also conferred enhanced gravity bending ability to the transgenic roots (P<0.001, Student t test; Fig. 6C). Therefore, the auxin-related phenotypes of *ZIFL1.1*-overexpressing lines were strikingly opposite to those uncovered for the *zifl1* mutants. By contrast, overexpression of *ZIFL1.3* had no effect on any of these auxin-related processes. However, while no change in the transpiration potential of *ZIFL1.1*-overexpressing leaves was detected, leaves from *ZIFL1.3*-overexpressing plants exhibited significantly lower transpiration rates than those of the wild type (Fig. 6D). Consistent with this and contrarily to the *zifl1* mutants, *ZIFL1.3*-overexpressing plants noticeably closed their stomata more efficiently than wild-type or *ZIFL1.1*-overexpressing plants, irrespective of the condition tested (Fig. 6E). Finally, the *ZIFL1.2*-overexpressing lines, which were included in all the phenotypical assays performed, did not exhibit any evident phenotype (Figs. 6A-D and S2B), indicating that this *ZIFL1*-specific transcript has no function, at least in the parameters tested.

To unequivocally ascertain ZIFL1.1 and ZIFL1.3 functional specificity, we then assessed the ability of these isoforms to suppress the *zifl1* mutant defects by phenotyping the transgenic lines expressing either the ZIFL1.1-GFP or the ZIFL1.3–GFP fusion protein under the control of the *ZIFL1* promoter in the *zifl1-1* and *zifl1-2* mutant backgrounds. As depicted in Table 1, complementation with ZIFL1.1-GFP fully abolished the PR elongation hypersensitivity to exogenous auxins of the *zifl1* mutants, but had no effect on their water loss rates. Conversely, ZIFL1.3-GFP fully complemented the drought-related phenotype, but not the auxin-related defects. In addition to demonstrating that the GFP fusion proteins are functionally active, these results, together with those from the overexpression studies, provide evidence that the two alternative ZIFL1 splice isoforms have distinct biological functions, with ZIFL1.1 modulating root auxin-related processes and ZIFL1.3 regulating drought stress tolerance.

ZIFL1.1 Influences Cellular Auxin Efflux in Yeast and *Arabidopsis*

The opposite alterations conferred by loss and gain of *ZIFL1.1* function in auxin-related processes led us to hypothesize that this isoform regulates auxin transport in the *Arabidopsis* root. In a previous study, we reported that heterologous expression of the ZIFL1.3 isoform confers enhanced 2,4-D and IAA resistance in *S. cerevisiae*, most likely sustained by an increased efflux from the yeast cell, at least in the case of 2,4-D (Cabrito

et al., 2009). We therefore decided to reexamine the auxin transport activity of ZIFL1.3 in parallel to that of ZIFL1.1 in the yeast Δ*tpo1* mutant, which lacks an MFS transporter involved in 2,4-D and IAA resistance (Teixeira and Sá-Correia, 2002). Correct expression of the GFP-ZIFL1.1 and GFP-ZIFL1.3 fusion proteins was confirmed by western blotting (Fig. S4A). Subcellular localization studies showed that both plant isoforms are targeted to the yeast plasma membrane (Fig. S4B), in agreement with the localization observed *in planta* for the ZIFL1.3 but not for the ZIFL1.1 isoform (see Fig. 3). The latter observation is not so surprising, as plant proteins, particularly transporters, may not always be targeted properly when expressed in yeast (Bassham and Raikhel, 2000). We took advantage of ZIFL1.1 mislocalization, as plasma-membrane targeting is a prerequisite to study ZIFL1 transport properties in the Δ*tpo1* background (Cabrito et al., 2009). As seen in Figure S4C, Δ*tpo1* mutant cells expressing GFP-ZIFL1.1 or GFP-ZIFL1.3 similarly exhibited higher final biomass and a reduced lag phase in the presence of 2,4-D or IAA. This enhanced resistance was correlated with a significant reduction in the accumulation of [^{14}C]-2,4-D or [^{14}C]-IAA in non-adapted yeast Δ*tpo1* cells suddenly exposed to either radiolabeled auxin (Table 2). As compared with yeast cells harboring the empty vector, net auxin accumulation was reduced by approximately 50% in cells expressing either of the two plant isoforms, indicating that ZIFL1.1 and ZIFL1.3 mediate similar auxin transport activity, at least in *S. cerevisiae*. In agreement with previous reports in yeast heterologous systems, Figure 7A shows that the IAA accumulation rate was reduced by about 30% when cells were challenged with the polar auxin efflux inhibitor naphthylphtalamic acid (NPA), probably owing to the inhibitory effect this chemical exerts on endogenous yeast transporters (Geisler et al., 2005; Yang and Murphy, 2009). However, this negative effect was not further intensified by expression of either plant isoform, indicating that the IAA transport activity mediated by ZIFL1.1 and ZIFL1.3 is not inhibited by NPA in *S. cerevisiae*.

We next investigated whether the ZIFL1.1 and ZIFL1.3 transporters also influence cellular auxin levels in *Arabidopsis* using a radiolabeled auxin accumulation assay in excised root tips. The results presented in Table 2 show that the saturable accumulation of both [^{14}C]-2,4-D and [^{14}C]-IAA was increased in *zifl1* mutant root tips when compared with the wild type or *ZIFL1.3*-overexpressing lines, whereas accumulation levels were slightly but significantly reduced by *ZIFL1.1* overexpression. As observed with the PR elongation assays (see Fig. 5A and 5B; Table 1), the measured effects were more pronounced when

assessing 2,4-D than IAA accumulation. In addition, all types of root tips displayed wild-type levels of NAA accumulation, consistent with the wild-type responsiveness of their PRs to this synthetic auxin analog (see Fig. S3). As the saturable amount of auxin retained in the root tip reflects the balance between cellular influx and efflux of auxin, we then measured the net efflux from root tips pre-loaded with labeled IAA. Figure 7B shows that *zifl1* mutant root tips accumulated more IAA due to decreased efflux, whereas *ZIFL1.1*-overexpressing lines accumulated less auxin as a result of higher IAA efflux rates, indicating that ZIFL1.1 influences cellular IAA efflux at the root apex.

ZIFL1.1 Modulates Polar Auxin Transport in the *Arabidopsis* Root

Given the encouraging results described above, we next aimed at determining whether the ZIFL1.1 transporter plays a role in the polar transport of IAA in roots. To this end, we first examined the effect of different chemical inhibitors of polar auxin transport on the elongation of *zifl1*-mutant and *ZIFL1.1*-overexpressing PRs (Table 3). While both root types responded to the auxin influx inhibitor naphthyoxyacetic acid (NOA) as the wild type, mutant and *ZIFL1.1*-overexpressing lines exhibited enhanced and reduced resistance, respectively, to the inhibitory effect that the auxin efflux inhibitors NPA and triiodobenzoic acid (TIBA) exert on PR elongation (Chen et al., 1998; Luschnig et al., 1998). These data reinforce the notion that ZIFL1.1 influences exclusively cellular auxin efflux, hinting at its involvement in polar auxin transport. By contrast, *ZIFL1.3*-overexpressing lines behaved as the wild type in this assay, further supporting the finding that the ZIFL1.3 truncated isoform plays no role in auxin-related processes.

To validate our hypothesis at the whole-plant level, we indirectly visualized auxin distribution by histochemical staining of wild-type and *zifl1*-mutant root tips carrying the well-described *ProDR5:GUS* auxin-responsive reporter construct (Ulmasov et al., 1997; Delker et al., 2010). Under control conditions, DR5 activity in both types of roots was confined to a small collection of cells comprising the quiescent center and the stem cell niche (Figs. 7C and S5), as previously reported (Sabatini et al., 1999). Localized application of IAA at either the hypocotyl-root junction or the extreme root tip of wild-type and *zifl1* mutant roots similarly led to a substantially more robust staining in these particular cell types. In addition, in the wild-type background GUS staining further extends into the distal elongation zone, with a clear gap in the region spanning from the quiescent

center to the transition zone. By contrast, when IAA was applied at the hypocotyl-root junction of *zifl1* mutant roots, staining barely spread into the apical meristem, with little if any staining evident in the transition or distal elongation zones. The DR5 activity pattern of the *zifl1* mutants was also considerably distorted after root-tip localized IAA treatment, with staining expanding from the quiescent center into the elongation zone without a well-defined boundary between the apical meristematic and distal elongation zones (Fig. 7C). The latter phenomenon was reproducibly observed when IAA was applied at a lower concentration at the root apex (Fig. S5). These observations strongly suggest that ZIFL1.1 function facilitates shootward auxin redistribution from stem cells of the extreme root apex to mature cells of the distal elongation zone. Indeed, auxin distribution is at least qualitatively similarly distorted by mutations in the auxin efflux carrier PIN2, an established regulator of root shootward auxin transport (Luschnig et al., 1998; Shin et al., 2005).

The relevance of ZIFL1.1 function to shootward auxin transport was further assessed by directly measuring IAA transport rates in both polarities using the optimized whole-root assay described by Lewis and Muday (2009). As PIN2 is one of the IAA efflux carriers sustaining shootward auxin transport in the root (Chen et al., 1998; Müller et al., 1998), we included the *eir1-4* mutant, a null *pin2* allele in the Col-0 ecotype (Luschnig et al., 1998), in this analysis. The entire assay was also recapitulated replacing IAA by benzoic acid (BA) as a weak acid diffusion control (Table S1). As seen in Figure 7D, rootward transport rates in *eir1-4* and *zifl1-1* mutant roots were comparable to those of the wild type, remaining also unaffected by *ZIFL1.1*-overexpression. By contrast, the *eir1-4* mutant displayed as expected a pronounced but partial defect in root shootward IAA transport, which was reduced by approximately 30% when compared to the wild type, in agreement with previous reports (Luschnig et al., 1998; Rashotte et al., 2000). Noticeably, *zifl1*-mutant and *ZIFL1.1*-overexpressing roots showed significantly (around 14%) decreased and enhanced rates of shootward IAA transport, respectively, confirming that ZIFL1.1 plays a role in shootward auxin transport at the root tip. Furthermore, we found that, while impairing rootward transport rates to a similar extent in all root types, NPA treatment failed to inhibit shootward IAA transport rates in the *eir1-4* and *zifl1-1* mutants to the same extent as in the wild type, as already reported for the *eir1-4* mutant (Rashotte et al., 2000). Despite being slightly less pronounced in the *zifl1-1* than in the *eir1-4* mutant background, the opposite effect was observed in *ZIFL1.1*-overexpressing roots.

Together with the results from the PR elongation assay in presence of NPA (see Table 3), the data presented in Figure 7D demonstrate that ZIFL1.1-mediated IAA transport activity is NPA-sensitive in plant. In combination with its NPA-insensitivity in yeast (see Fig. 7A), this further suggests that the tonoplastic ZIFL1.1 transporter does not function as an auxin transporter itself, but rather favors shootward auxin flows driven by typical plasma-membrane IAA efflux carriers whose IAA export activity is inhibited by NPA in both plant and heterologous systems (Noh et al., 2001; Murphy et al., 2002; Petrasek et al., 2006; Yang and Murphy, 2009).

ZIFL1.1 function affects plasma-membrane PIN2 abundance

We then hypothesized that ZIFL1.1 function would play a role in fine-tuning polar IAA transport, particularly in situations of enhanced auxin fluxes, by modulating the activity of a specific auxin transporter. Given that ZIFL1.1 influences mainly if not exclusively cellular auxin efflux, a prime potential downstream target for this vacuolar MFS transporter was PIN2, hitherto the sole polarly localized auxin efflux carrier implicated in shootward transport in epidermal cells of the root meristematic and transition zone (Chen et al., 1998; Luschnig et al., 1998; Müller et al., 1998).

As discussed elsewhere (Petrasek and Friml, 2009; Löfke et al., 2013), carrier-mediated auxin transport can be altered by regulating a given transporter's abundance, subcellular trafficking or activity levels. Since an experimental design to measure PIN activity is still lacking, we focused on examining the distribution and steady-state levels of PIN2 at the plasma membrane by immunofluorescence labeling of its native protein at the PR tip (Fig. 8A). As expected, no PIN2 signal was detected in the *eir1-4* mutant background (Luschnig et al., 1998), whereas proper polar localization of PIN2 at the plasma membrane of wild-type root tips, i.e. shoowtard and rootward orientation in cells of the epidermis/lateral root cap and cortex, respectively (Müller et al., 1998; Boonsirichai et al., 2003; Rahman et al., 2007), was observed. This asymmetric subcellular distribution was unaltered upon prolonged IAA treatment, consistent with previous reports that the polarity of PIN2 localization is not auxin-responsive (Peer et al., 2004; Rahman et al., 2007). Importantly, even under IAA challenge, mislocalization of the auxin efflux carrier was not observed in either *ZIFL1.1* loss-of-function or overexpression lines, indicating that ZIFL1.1 function does not interfere with PIN2 polar targeting. However, in the presence of 0.1 µM IAA, PIN2

fluorescence levels appeared to be altered in the *ZIFL1* mutant and transgenic lines. We therefore assessed PIN2 abundance by quantifying the corresponding immunofluorescence signal at the plasma membrane of root tip epidermal cells (Fig. 8B). Under control conditions, PIN2 incidence at the cell surface was not altered by ZIFL1.1 function, as illustrated by the equivalent PIN2 levels detected in wild-type, *zifl1-1* mutant and *ZIFL1.1*-overexpressing root tips. In seedlings grown in the presence of IAA, a substantial reduction in PIN2 plasma-membrane abundance was detected in the wild type, consistent with PIN2 protein degradation following prolonged IAA treatments (Sieberer et al., 2000; Vieten et al., 2005; Abas et al., 2006; Kleine-Vehn et al., 2008a; Baster et al., 2012). Notably, we found that under IAA challenge PIN2 stability at the plasma membrane of root tip epidermal cells was significantly decreased and enhanced by *ZIFL1.1* loss-of-function and overexpression, respectively. These results are in clear agreement with the gathered physiological data (see Figs 5 and 6) and indicate that, in the context of a stronger polar IAA stream, activity of the ZIFL1.1 transporter influences the steady-state levels of PIN2 at the plasma membrane, further supporting the notion that ZIFL1.1 acts as a positive regulator of shootward auxin transport.

ZIFL1 Catalyzes Potassium and Proton-Coupled Transport Activities

In a first attempt to identify the physiological substrate(s) of the two plant ZIFL1 splice isoforms, we further examined the response of Δ*tpo1* mutant yeast cells expressing either GFP-ZIFL1.1 or GFP-ZIFL1.3 to various additional compounds. As seen in Figure S4D, expression of either GFP-ZIFL1.1 or GFP-ZIFL1.3 similarly conferred enhanced yeast resistance to two weak acids, malate and acetate, as well as to the metal ions Al^{3+} and Tl^{3+}, as already reported for the latter in the case of the ZIFL1.3 isoform (Cabrito et al., 2009). Hence, ZIFL1 is also able to modulate ion and weak acid sensitivity in yeast. Interestingly, we also found that expression of either *ZIFL1* splice variant dramatically increases yeast sensitivity to the metal ion Cs^+ (Fig. S4D). Cesium possesses similar chemical properties to potassium, and physiological studies in plants have demonstrated that Cs^+ competes with K^+ influx by entering root cells through at least some of the K^+ uptake systems (White and Broadley, 2000; Qi et al., 2008). We therefore decided to investigate whether the ZIFL1 transporter can also influence K^+ delivery to the yeast cell, by evaluating the capacity of the two ZIFL1 isoforms to rescue the deficient growth of the

551 Δ*qdr2* deletion mutant under limiting potassium concentrations (Vargas et al., 2007).
552 Figure 9A shows that both ZIFL1.1-GFP and ZIFL1.3-GFP were able to markedly alleviate
553 the pronounced growth defect induced by loss of Qdr2 at low K^+ concentrations. This
554 finding strongly suggests that both the *Arabidopsis* ZIFL1.1 and ZIFL1.3 isoforms possess
555 potassium transport activity.

556 Prompted by an earlier microarray study reporting *ZIFL1* induction upon plant exposure
557 to Cs^+ (Hampton et al., 2004), we next investigated whether ZIFL1 function affects PR
558 elongation in response to both K^+ and Cs^+ (Fig. 9B). Like the loss-of-function mutants,
559 *ZIFL1.1*-overexpressing plants responded as the wild type to the inhibitory effect induced
560 by K^+. However, in clear contrast to the hyper-resistance conferred by the *zifl1* mutations,
561 the *ZIFL1.1* transgenic line displayed decreased tolerance to inhibitory concentrations of
562 Cs^+ (Fig. 9B). This led us to examine LR formation in the presence of Cs^+. As shown in
563 Figure 9C, cesium induced the production of LR structures to a similar extent in wild-type,
564 *zifl1* mutant and *ZIFL1.1*-overexpression lines. Furthermore, the ratio between LR
565 primordia and emerged LRs was not significantly altered by either the mutations or
566 enhanced ZIFL1.1 levels, and the positive effect exerted by Cs^+ on LR elongation was also
567 similar in all genotypes (Fig. 9C). Therefore, the effects of loss and gain of *ZIFL1* function
568 on LR emergence are suppressed in presence of Cs^+, which along with the effects of its
569 own toxicity is perceived by root cells as a potassium deficiency (Hampton et al. 2004).
570 These results thus indicate that ZIFL1.1 may play a role in Cs^+ and/or K^+ homeostasis in
571 plant root cells.

572 As MFS transporters are believed to function mainly as proton-motive-force-driven
573 secondary transporters, catalyzing uniport, symport or antiport activities (Pao et al., 1998),
574 we analyzed the proton-dependence of ZIFL1.1 and ZIFL1.3 activity in yeast. The
575 intracellular pH regulation is essentially sustained in *S. cerevisiae* by the action of the
576 plasma membrane H^+-ATPase Pma1 (Serrano, 1978). As the activity of this proton pump
577 and the passive proton influx through the yeast plasma membrane can be estimated by
578 monitoring the pH of the external medium, we compared the acidification curves of Δ*qdr2*
579 cells expressing the two plant transporters under growth-limiting potassium conditions.
580 Low potassium levels were previously shown to lead to a reduced rate of extracellular
581 medium acidification by yeast cells lacking Qdr2 when compared to the wild-type strain
582 (Vargas et al., 2007). Importantly, expression of either the GFP-ZIFL1.1 or GFP-ZIFL1.3

fusion proteins was found to increase the rate of H^+ efflux in Δ*qdr2* cells grown in medium with low potassium (Fig. 9D), demonstrating that the two *Arabidopsis* transporters influence proton transport across the plasma membrane of yeast cells challenged with potassium deprivation.

Finally, to investigate whether the ZIFL1.1 isoform is also involved in proton transport activity in *Arabidopsis*, we assessed vacuolar acidification in root tips using an acidification marker, the dye acridine orange. As seen in Figure 9E, acidification of the central vacuoles was notably enhanced in *zifl1-1* mutant roots, while *ZIFL1.1*-overexpressing seedlings exhibited a considerable reduction in root vacuolar acidification when compared to the wild type. These results strongly suggest that ZIFL1.1 mediates proton efflux from the vacuolar compartment in *Arabidopsis* root tip cells.

DISCUSSION

Alternative Splicing Determines a Dual Function for the ZIFL1 Transporter

The present work reveals a previously unrecognized role for an MFS transporter in modulating both polar auxin transport and stomatal movements. In fact, a key finding of this study is that alternative splicing determines a dual function for the *Arabidopsis* ZIFL1 transporter, with the full-length ZIFL1.1 and the truncated ZIFL1.3 proteins regulating polar auxin transport and drought tolerance, respectively, as demonstrated by the exclusive ability of the corresponding GFP-tagged isoforms to rescue two distinct phenotypes displayed by *zifl1* insertion mutants. Proof of such a double function also stems from our overexpression studies, which further show that while both the *ZIFL1.1* and *ZIFL1.3* splice variants code for functional membrane transporters, the remaining alternative transcript, *ZIFL1.2*, may either not be translated or encode a transporter with no function, at least in the biological processes analyzed.

Alternative splicing, which generates multiple transcripts from the same pre-mRNA, is an important generator of proteomic diversity and functional complexity in higher eukaryotes. Despite the fact that over 60% of the *Arabidopsis* multiexon genes are currently estimated to undergo alternative splicing (Marquez et al., 2012), information on the functional significance of this key post-transcriptional regulatory mechanism in plants is surprisingly scarce, having been uncovered for only about a dozen genes (Carvalho et al.,

2012). We report here a compelling example of the functional impact of alternative splicing, which by dictating the subcellular and tissue distribution of two splice forms allows the same gene to fulfill strikingly different biological roles in *Arabidopsis*.

The *ZIFL1.3* transcript arises from selection of an alternative 3' splice site, causing a frame-shift mutation that results in the production of an MFS protein lacking the two last C-terminal membrane-spanning domains. We found that this splicing event directs dual targeting of the ZIFL1 transporter, with the full-length ZIFL1.1 isoform localizing to the tonoplast, while the truncated ZIFL1.3 isoform is addressed to the plasma membrane. On the other hand, the two splice forms possess strikingly similar activities when heterologously expressed in yeast, suggesting that the region absent from the ZIFL1.3 protein influences mainly its subcellular localization *in planta* but not its substrate specificity or transport activity, at least when secluded from the plant system. The only other report of plant splice variants clearly fulfilling distinct functions is that of the *Arabidopsis* SR45 splicing factor, with SR45.1 playing a role in flower petal development and SR45.2 being required for normal root growth (Zhang and Mount, 2009). However, while both *SR45* transcripts are ubiquitously expressed in plant tissues, we were able to detect the endogenous *ZIFL1.3* transcript only in leaf and not in root tissues. Moreover, the ZIFL1.3-YFP fusion is undetectable in root tissues, whereas the ZIFL1.1-YFP fusion is observed at high levels in root cell vacuolar membranes. This suggests that tissue-specific factors differentially affect *ZIFL1* pre-mRNA processing and/or splice variant stability in leaves and roots. Identification of the precise molecular mechanisms controlling the tissue distribution of the *ZIFL1* transcripts is beyond the scope of this study, but represents an exciting avenue of future work.

Unfortunately, although the GFP-tagged ZIFL1.3 isoform is functionally active, we were unable to visualize it in leaf stomatal guard cells where significant *ZIFL1* promoter activity is detected. Most transporters or channels are present at very low copy numbers in this particular cell type and can hardly be visualized using their own promoter (Nagy et al., 2009; Meyer et al., 2010). Nevertheless, the unique ability of the ZIFL1.3 isoform to reduce transpiration rates by regulating stomatal movements, which is in agreement with the description of *ZIFL1* as a signature gene in three different *Arabidopsis* ecotypes exposed to elevated ambient CO_2 levels (Li et al., 2006), along with the subcellular localization observed in protoplasts and tobacco cells strongly support the notion that this isoform

indeed resides at the guard-cell plasma membrane. The restricted ZIFL.3 functionality also confirms the absence of a link between the root and drought phenotypes. In this respect, ZIFL1 function resembles that of the *Arabidopsis* Multidrug-Resistance associated Protein (MRP) ABCC5, which confers partial drought insensitivity upon water stress by regulating stomatal apertures, but also controls PR elongation and branching (Gaedeke et al., 2001; Suh et al., 2007). In a subsequent study, Nagy et al. (2009) elegantly demonstrated that guard-cell targeted expression of ABCC5 partially relieves the defective stomatal responses of the corresponding null mutant without rescuing its root phenotype. By contrast, the ability of the *Arabidopsis* vacuolar H^+-pyrophosphatase AVP1 to withstand drought stress clearly correlates with its positive effect on root development through the facilitation of auxin fluxes (Li et al., 2005; Park et al., 2005).

ZIFL1.1 Participates in Auxin Efflux during Root Shootward Transport

Importantly, by directly measuring root IAA transport rates in both polarities and by indirectly visualizing auxin maxima in the root tip, we demonstrate that the full-length ZIFL1.1 transporter participates in shootward auxin redistribution from the apex to the elongation zone in the *Arabidopsis* root. Accordingly, many if not all aspects of the pleiotropic phenotypes caused by loss and gain of *ZIFL1.1* function are consistent with impaired shootward auxin transport, which is actually sufficient to sustain both PR elongation and gravitropic bending (Rashotte et al., 2000). A role in shootward auxin transport is also in agreement with the particularly strong ZIFL1.1 expression detected in the epidermal cell layer of the root apical meristem and the transition zone, where shootward localization of the auxin carriers AUX1 and PIN2 has been demonstrated to control shootward auxin movement and hence root gravitropism (Swarup et al., 2005; Wisniewska et al., 2006). Interestingly, the ZIFL1.1 transporter is also highly expressed in root meristematic cortical cells, where rootward localization of PIN2 is required for an optimal gravitropic response (Rahman et al., 2010). More puzzling is the finding that ZIFL1.1 function is specifically required at the emergence phase of LR formation — firstly because the auxin shootward stream in the PR promotes LR initiation rather than emergence (Wu et al., 2007), and secondly because the *ZIFL1* promoter is strongly activated in the LR but only after emergence. A recent study showed that increased activity of the auxin influx carrier LAX3 in cortical and epidermal cells directly overlaying

new LR primordia promotes LR emergence, likely by reinforcing the auxin-dependent localized induction of a subset of cell-wall remodeling enzymes that are crucial for cell wall separation at this step (Swarup et al., 2008). In addition, the effect that ZIFL1.1 exerts on LR elongation may result mainly from the auxin transport it mediates in the LR itself, as previously shown for the auxin efflux carrier ABCB1 (Wu et al., 2007).

The opposite alterations in auxin inhibition of PR elongation caused by loss and gain of *ZIFL1.1* function are consistent with a role in root cellular auxin efflux. Indeed, mutations in a transporter influencing auxin influx would be expected to confer reduced auxin sensitivity, in agreement with the impaired ability of the corresponding mutant to accumulate inhibitory levels of auxin, as shown for the AUX1 influx carrier (Bennett et al., 1996). By contrast, nearly all auxin efflux carrier mutants over-accumulate auxin at the root tip and are consequently more sensitive to exogenous auxins (Chen et al., 1998; Luschnig et al., 1998; Lin and Wang, 2005; Terasaka et al., 2005). Accordingly, loss of *ZIFL1* function respectively enhances and reduces auxin accumulation and efflux activity of excised root segments. The correlation between these phenotypes and root transport activity is not only qualitative but also quantitative, as both aspects are more pronounced in the presence of the synthetic auxin 2,4-D than of the naturally-occurring IAA. These data were complemented by assessing the sensitivity of the different genotypes to polar auxin influx and efflux inhibitors. Importantly, only the auxin efflux inhibitors NPA and TIBA induce a differential PR response, with *zifl1* mutants and *ZIFL1.1*-overexpression lines displaying respectively enhanced resistance and sensitivity to these compounds, as shown previously for numerous auxin efflux mutants (Chen et al., 1998; Luschnig et al., 1998; Lin and Wang, 2005). An apparent discrepancy with the proposed model regards the results obtained using the two synthetic auxins 2,4-D and 1-NAA, which have been employed experimentally to distinguish between IAA import and efflux activities, respectively (Delbarre et al., 1996; Yamamoto and Yamamoto, 1998). Rather unexpectedly, in PR elongation and root accumulation assays, no effect of loss of *ZIFL1* function was found for 1-NAA, while hypersensitivity was observed for 2,4-D. However, Luschnig et al. (1998) also reported the absence of a discernible effect of 1-NAA on PR elongation of the *eir1-4* mutant. On the other hand, a role in auxin influx should result in enhanced resistance, not sensitivity, of the *zifl1* mutants to 2,4-D. Furthermore, while it is known that 2,4-D is poorly transported in a polar fashion, it can also constitute a weak substrate of key auxin efflux

carriers among both ABCBs and PINs (Yang and Murphy, 2009). As this auxin significantly induces *ZIFL1* expression (Cabrito et al., 2009), it is conceivable that the plant takes advantage of the ZIFL1.1 role in auxin transport to reallocate this function to xenobiotic resistance.

The Tonoplastic ZIFL1.1 Transporter Assists in Polar Auxin Transport

Several lines of evidence indicate that ZIFL1.1 modulates auxin transport indirectly. First, a tonoplast-localized transporter cannot directly catalyze auxin efflux at the plasma-membrane, and though IAA conjugates and IBA provide a readily available pool of free IAA upon hydrolysis in the ER lumen or β-oxydation in the peroxysomes, respectively (reviewed in Woodward and Bartel, 2005), storage or compartmentalization of such compounds in the vacuole has not been reported. Secondly, *zifl1* mutants exhibit only subtle changes in root gravitropism and PR elongation sensitivity to exogenous auxins, which are attributable to minor alterations in shootward auxin transport at the root tip. Moreover, apart from PR branching, *zifl1* mutants fail to display morphological alterations under normal conditions, where the large majority of the described auxin efflux mutants exhibit specific defects in PR and/or gravitropic growth (Chen et al., 1998; Luschnig et al., 1998; Noh et al., 2001; Lin and Wang, 2005; Terasaka et al., 2005). Last but not least, ZIFL1.1 activity is NPA-sensitive *in planta* but NPA-insensitive in yeast. Our heterologous expression studies show that ZIFL1.1 is able to mediate IAA transport in yeast cells without requiring additional plant-specific factors. Indeed, transport activity of plant auxin carriers can be demonstrated in various heterologous systems (Geisler et al., 2005; Yang et al., 2006; Blakeslee et al., 2007; Yang and Murphy, 2009), but the activation of other endogenous transporters catalyzing auxin efflux cannot always be ruled out. We found that NPA inhibition of yeast IAA transport activity is unaffected by expression of the ZIFL1.1 transporter, while *in planta* NPA treatment fails to reduce shootward transport in the *zifl1-1* mutant to the same extent as in the wild type. The latter observation, which is even more evident in the *eir1-4/pin2* mutant background (this study; Rashotte et al., 2000), suggests that, by reducing shootward auxin transport rates, absence of the carrier attenuates sensitivity to the auxin efflux inhibitor. Indeed, in contrast with ZIFL1.1, PIN2-mediated IAA export activity in yeast and other heterologous systems is clearly NPA-sensitive (Petrasek et al., 2006; Blakeslee et al., 2007; Yang and Murphy, 2009).

We further propose that fine-tuning of polar IAA efflux by ZIFL1.1 relies on a protective effect on PIN2 plasma-membrane stability under conditions of high IAA flow that normally trigger PIN2 degradation. Recent studies have established auxin as the main regulator of its own asymmetric distribution (reviewed in Löfke et al., 2013). Dynamic polar sorting of PINs at the plasma membrane is sustained by repeated steps of endocytotic internalization and recycling back to the plasma membrane via exocytosis (Geldner et al., 2001; Dhonukshe et al., 2007). This constitutive cycling of PIN proteins controls not only their subcellular localization, but also their plasma-membrane abundance (Kleine-Vehn et al., 2008b). While physiological IAA concentrations inhibit the internalization step of PIN2 cycling promoting its stability at the plasma membrane (Paciorek et al., 2005), extended treatments with high IAA concentrations trigger PIN2 protein degradation through lytic vacuolar targeting and proteasomal activity, thus reducing its plasma-membrane incidence (Sieberer et al., 2000; Kleine-Vehn et al., 2008a; Laxmi et al., 2008). The combination of these auxin antagonistic effects on intracellular trafficking and proteasome-mediated degradation allows the positional control of PIN2 activity sustaining root gravitropism (Abas et al., 2006; Baster et al., 2012). As the vacuolar ZIFL1.1 transporter does not appear to affect PIN2 polar distribution, it is tempting to speculate that ZIFL1.1 activity modulates PIN2 steady-state levels at the plasma membrane by interfering with its vacuolar targeting and/or degradation, as already reported for the Modulator of PIN (MOP) regulators (Malenica et al., 2007). At present, we cannot exclude the possibility of a more general effect on auxin efflux, as PIN2-mediated shootward auxin transport has been shown to be supported for instance by the action of ABCB4 (Terasaka et al., 2005; Lewis et al., 2007). On the other hand, ZIFL1.1 activity could also influence PIN2 activity levels, namely through changes in plasma-membrane electrochemical potential. In fact, our yeast extracellular and plant vacuolar acidification assays indicate that ZIFL1.1 may facilitate polar auxin transport by enhancing the release of protons from the vacuole, thus increasing H^+ availability for plasma-membrane ATPases and the proton-driving force for cellular auxin transport. Interestingly, AVP1 has been shown to promote auxin-mediated organ development by influencing apoplastic acidification through its action on the abundance and activity of the plasma membrane P-ATPase and by directly affecting trafficking or stability of the PIN1 carrier (Li et al., 2005).

Potassium as the Physiological Substrate of the ZIFL1 Transporter

The identification of the physiological substrate of a membrane transporter is of prime importance in dissecting the precise molecular mechanisms underlying its function. Our yeast experiments show that the effect of ZIFL1 expression is not restricted to auxins, influencing also the response to other weak acids and a few ions. Interestingly, ZIFL1 markedly increases yeast sensitivity to Cs^+. Results obtained by Hampton et al. (2004) indicate that the main effect that cesium induces in plants along with its own toxicity is potassium starvation. In support of this notion, complementation experiments with the Δ*qdr2* yeast mutant indicate high-affinity K^+ transport activity for both ZIFL1 splice isoforms. Indeed, potassium fluxes, in particular those mediated by K^+ channels, have been previously shown to modulate auxin-induced cell elongation growth (Christian et al., 2006; Fuchs et al., 2006). Moreover, deletion of the *Arabidopsis* K^+ carrier TRH1 leads to auxin-related phenotypes similar to those reported here for the *zifl1* mutants (Vicente-Agullo et al., 2004). Although the molecular mechanisms governing TRH1-dependent auxin transport remain unknown, this unexpected function of the potassium carrier was suggested to rely on its ability to generate ionic and electric gradients across the plasma membrane that favor auxin efflux through specific transporters (Vicente-Agullo et al., 2004), as proposed here for the ZIFL1.1 transporter. Cesium suppression of the LR emergence and elongation effects along with the altered PR elongation in response to cesium caused by altered ZIFL1.1 levels provide a first link between the potassium and auxin transport activities of this MFS carrier. The *Arabidopsis* Nitrate Transporter NRT1.1 has been recently proposed to repress LR growth at low nitrate availability by promoting shootward auxin transport out of these roots, thus connecting nutrient sensing and auxin-dependent developmental adaptation (Krouk et al., 2010). Interestingly, *ZIFL1* expression appears to be highly repressed in the *nrt1.1* knockout background (Munos et al., 2004).

Finally, the notion of K^+ as the physiological substrate of the ZIFL1 MFS transporter is also consistent with ZIFL1.3's function in the regulation of stomatal movements, since potassium fluxes are well-established regulators of guard cell turgor in response to endogenous and environmental cues (Ward et al., 2009). Nagy et al. (2009) showed that ABCC5 possesses high-affinity *myo*-inositol hexa*kis*phosphate transport activity, thus linking this substrate to a pleiotropic function in PR elongation, seed mineral cation and phosphorus status regulation, stomatal aperture control and drought stress tolerance. The

present study provides compelling evidence that the two splice isoforms of the ZIFL1 MFS carrier share K^+ transport activity likely to influence membrane proton gradients, and that their distinct biological roles stem solely from their different subcellular and tissue distribution.

METHODS

Plant Materials and Growth Conditions

The *Arabidopsis thaliana* Colombia (Col-0) ecotype was used as the wild type in all experiments. Seeds of the T-DNA insertion mutants *zifl1-1* (SALK_030680) and *zifl1-2* (GABI_052H08) were obtained from NASC (Nottingham, UK). The exact T-DNA insertion sites were confirmed using gene-specific primers (Table S2) and primers annealing at the T-DNA borders, which also allowed PCR-based genotyping to identify homozygous lines.

Plant transformation was achieved by the floral-dip method (Clough and Bent, 1998) using *Agrobacterium tumefaciens* strain EHA105. Highly similar results were obtained following extensive characterization of all transgenic lines generated for each construct, and representative results for one line are presented.

Seeds were surface-sterilized, sown on Murashige and Skoog (1962) medium solidified with 0.8% agar, stratified at 4°C for 3 d in the dark, and placed in a growth chamber where they were transferred to soil after 2-3 weeks. All phenotypical assays were performed in a climate-controlled growth cabinet. Plants were cultivated either under 16-h light/8-h dark (long-day) or 8-h light/16-h dark (short day) conditions at 23°C (light period)/18°C (dark period) and 60% RH. Hormones, antibiotics and other compounds were purchased from Sigma (St. Louis, USA).

Gene Expression and Sequencing Analyses

RT-PCR analyses were performed as previously described (Remy et al., 2012) using primers designed to detect *ZIFL1*, *ROC10* and *UBQ10* expression (Table S2). For native *ZIFL1* promoter reporter gene experiments, a fragment including the 1778 bp immediately upstream of the first start codon was PCR-amplified (Table S2) from genomic DNA and inserted via the *Sac*I/*Sac*II restriction sites into the pKGWFS7 plasmid (Karimi et al., 2002). After agroinfiltration of the resulting *ProZIFL1:GUS:GFP* construct into wild-type

plants, 13 independent transformants were recovered. For synthetic DR5 promoter reporter gene experiments, wild-type and *zifl1* mutant plants were transformed with the *ProDR5:GUS* construct inserted in the pEarleyGate301 vector (Ulmasov et al., 1997; Earley et al., 2006; Delker et al., 2010), and six independent transformants per genotype were isolated. Histochemical staining of GUS activity was performed as described by Sundaresan et al. (1995).

Sequencing analyses were performed on a 3130*x*/ Genetic Analyzer using the BigDye® Terminator v1.1 Cycle Sequencing Kit according to the manufacturer's instructions (Applied Biosystem, Carlsbad, USA).

Phenotypical Assays

Water loss assays were performed on irrigated non-bolting plants by weighing either detached entire rosette or four rosette leaves at various time intervals at room temperature (~22°C). Stomatal closure assays were performed as described by (Bright et al., 2006), with more than 60 apertures recorded per treatment. PR elongation assays and LR parameter evaluation were carried out as previously described (Remy et al., 2012). LR primordial stages were scored under the microscope and defined according to Malamy and Benfey (1997). For hypocotyl elongation assays, seeds were sown directly on control or auxin-containing medium plates set in the vertical position, stratified and grown for 5 d in the dark. For root tip reorientation assays, 5-d-old seedlings grown vertically on control medium were transferred to fresh medium and allowed to grow for an additional 2 d. Plates were then rotated 90°C anticlockwise and kept in the dark before the angle of root tips from the vertical plane was scored. Stomatal apertures, PR and hypocotyl elongation, LR length and root deviation angles were measured on scanned images using the ImageJ software (http://rsbweb.nih.gov/ij/).

Subcellular Localization Studies

To generate the ZIFL1-YFP and ZIFL1-GFP fusions, each *ZIFL1* transcript was PCR-amplified (Table S2) using root (*ZIFL1.1* and *ZIFL1.2*) or leaf (*ZIFL1.3*) cDNA as a template and independently inserted via the *Xho*I/*Pac*I restriction sites into the YFP- or GFP-tagged versions of the pBA002 vector. *Arabidopsis* protoplasts were generated as described by Yoo et al. (2007), transfected with the YFP constructs by polyethylene glycol

transformation (Abel and Theologis, 1994) and analyzed by confocal microscopy. Transient co-expression of the GFP constructs with the tonoplast marker γ-Tonoplast Intrinsic Protein (TIP)-mCherry or the plasma membrane marker Plasma membrane Intrinsic Protein 2A (PIP2A)-mCherry (Nelson et al., 2007) and the pBIN-NA construct (Silhavy et al., 2002) in leaf abaxial epidermal cells of *Nicotiana tabacum* was performed via the agroinfiltration procedure described by Voinnet et al. (2003) using *A. tumefaciens* strain GV3101.

For generation of stable transgenic lines, the 35S promoter in the *pBA002:ZIFL1.1-GFP* and *pBA002:ZIFL1.3-GFP* plasmids was replaced with the *ZIFL1* promoter. For each construct, six transgenic lines were recovered upon transformation of *zifl1-1* or *zifl1-2* mutant plants.

Genomic Complementation and Overexpression Analyses

For genomic complementation, a 5599-bp fragment encompassing the entire *ZIFL1* gene and including the 1778-bp promoter sequence described below was PCR-amplified (Table S2) from genomic DNA and inserted into the promoterless version of the pBA002 vector via the *Hind*III/*Xba*I restriction sites. The corresponding construct was introduced into *zifl1-1* and *zifl1-2* mutant plants, with three complementation lines being recovered for each mutant allele.

ZIFL1 overexpression constructs were obtained as described for the YFP plasmids, except that the corresponding fragments were inserted via the *Xho*I/*Asc*I restriction sites into the pBA002 background. After agroinfiltration of wild-type plants, three transgenic lines independently overexpressing each *ZIFL1* transcript were selected.

Yeast Experiments

The parental *S. cerevisiae* strain BY4741 (*MATa, his3Δ1, leu2Δ0, met15Δ0, ura3Δ0*) and the derived deletion mutants BY4741_Δ*tpo1* (*MATa, his3Δ1, leu2Δ0, met15Δ0, ura3Δ0, YLL028w::kanMX4*) and BY4741_Δ*qdr2* (*MATa, his3Δ1, leu2Δ0, met15Δ0, ura3Δ0, YIL121W::kanMX4*) were used in this study. The *Arabidopsis ZIFL1.1* and *ZIFL1.3* coding sequences were cloned into the pGREG576 vector (Jansen et al., 2005), and expression of the corresponding GFP fusion proteins was tested by western blotting and fluorescence microscopy analyses, as described in Cabrito et al. (2009). Strains and vector were

acquired from the Euroscarf collection (Frankfurt, Germany). Susceptibility and spot assays were carried out as described previously (Cabrito et al., 2009) in minimal growth MMB-U liquid and agarized medium, respectively. To test the chemical stress inducers, 2,4-D, IAA, CsCl, $Al_2(SO_4)_3$, $TlCl_3$, L-malic acid and acetic acid stock solutions (pH was adjusted to 4 for the weak acids) were added at the specified concentration. Growth under K^+ limitation was evaluated on agarized ammonium phosphate basal medium (KNA) supplemented with 0.2 or 2 mM KCl as previously described (Vargas et al., 2007). Auxin accumulation assays were carried out as in Cabrito et al. (2009), using 0.3 mM/0.5 mM of cold 2,4-D/IAA (Sigma) and 0.5 µM/0.5 µM of [^{14}C]-labeled 2,4-D/IAA (American Radiolabeled Chemicals, St. Louis, USA) in the absence or presence of NPA (10 µM). To compare the *in vivo* active export of protons, the external medium pH was monitored as in Vargas et al. (2007) using liquid KNA medium supplemented with 0.5 mM of KCl.

Auxin Transport Assays

Radiolabeled-auxin accumulation was assayed in root-tip segments as described by (Ito and Gray, 2006), except that radiolabeled auxins were used at a final concentration of 4.5 µM [^{14}C]-IAA (50 mCi/mmol), 7.5 µM [^{14}C]-2,4-D (50 mCi/mmol) or 0.3 µM [^{14}C]-NAA (10 mCi/mmol) (American Radiolabeled Chemicals). To examine [^{14}C]-IAA efflux, the same protocol was applied, except that after the 1-h incubation period, root tips were rinsed with three changes of uptake buffer, and further incubated in this buffer for 1 h before harvesting.

Rootward and shootward root auxin transport was assayed as described by Lewis and Muday (2009). After treatment with either 100 nM [^{3}H]-IAA or [^{3}H]-BA (American Radiolabeled Chemicals) applied as agar droplets for 13 h at the hypocotyl-root junction (rootward) or for 5 h at the root tip (shootward), 5-mm segments from the root apex (rootward) or spanning from 2 to 7 mm from the root tip (shootward) were excised.

Immunofluorescence Protein Localization Studies

For PIN2 immunofluorescence localization assays, 3-d-old seedlings grown vertically on control medium were transferred to fresh medium supplemented or not with 0.1 µM IAA and allowed to grow for an additional 2 d. Whole-mount immunolocalization in *Arabidopsis* roots was performed as described previously (Sauer et al., 2006). Rabbit anti-PIN2

primary antibody was used at a dilution of 1:1000 and fluorochrome-conjugated anti-rabbit-CY3 secondary antibody (Dianova GmbH, Hamburg, Germany) was diluted 1:600.

Microscopy

Differential interference contrast and confocal images were taken with a DM LB2 microscope (Leica, Germany) and an LSM 510 or 710 laser scanning microscope equipped with a Meta detector (Zeiss, Germany), respectively. For cell wall staining, roots were incubated in 10 µg/mL iodide propidium for 10 min. Acridine orange staining was performed as described by Hirano et al. (2011). Fluorescence detection parameters (laser intensity, offset, gain and pinhole settings) were set so that the fluorescence signal emitted by *zifl1-1* mutant root tips was just below the saturation threshold. All micrographs were acquired using identical fluorescence parameters to allow comparison with wild-type and *ZIFL1.1*-overexpressing root tips. Post-imaging, average fluorescence intensity of seven epidermal cells within a single file located 600 µm from the root apex was recorded. For PIN2 immunofluorescence signal quantification, at least seven root tip micrographs per genotype per condition were captured using identical confocal settings. Post-imaging, average fluorescence intensity of the PIN2 signal at the plasma membrane was recorded within each single epidermal cell file. Excitation wavelengths used to detect fluorescence were 488 nm for GFP and acridine orange, 514 nm for YFP, 543 nm for iodide propidium and mCherry, 458 nm for autofluorescence and 561 nm for CY3. Emitted fluorescence was monitored at detection wavelengths longer than 560 nm for iodide propidium and autofluorescence, between 565-615 nm for mCherry, between 535-590 nm for YFP and acridine orange, between 500-550 nm for GFP and between 569-649 nm for CY3.

Accession Numbers

Arabidopsis Genome Initiative locus identifiers for the genes mentioned in this article are as follows: *ZIFL1* (At5g13750), *ROC1* (At4g38740), *UBQ10* (At4g05320), *PIN2* (At5g57090), *γ-TIP* (At2g36830) and *PIP2A* (At3g53420).

Supplemental Data

Supplemental Figure S1. Sequencing Analysis of the *ZIFL1* Transcript Tissue Distribution.

Supplemental Figure S2. Auxin-related Hypocotyl Phenotype of *ZIFL1* Loss-of-Function Mutants and *ZIFL1*-overexpressing Lines.

Supplemental Figure S3. Effect of IBA and 1-NAA on the *zifl1-1* Mutant.

Supplemental Figure S4. Heterologous Expression of ZIFL1.1 and ZIFL1.3 in Yeast.

Supplemental Figure S5. Auxin-responsive *ProDR5:GUS* Expression in Wild-type and *zifl1* Mutant Roots.

Supplemental Table S1. Benzoic Acid (BA) Diffusion in Roots of the Wild Type, *eir1-4* and *zifl1-1* Mutants and *ZIFL1.1*-overexpressing Lines.

Supplemental Table S2. Sequences of Used Primers.

ACKNOWLEDGMENTS

We thank N.-H. Chua for the pBA002 vectors, T. Guilfoyle and M. Quint for the pEarley:DR5-GUS construct, M. Zeidler and D. Silhavy for the pBIN-NA plasmid, C. Luschnig for *eir1-4* mutant seeds and the anti-PIN2 antibody, R. Carvalho and V. Nunes for technical assistance, L. Boavida, M. Wudick and A. Rodrigues for helpful discussions, and M. Mallo, J. Feijó and E. Baena-González for comments on the manuscript. This work was funded by Fundação para a Ciência e a Tecnologia (Grants PTDC/AGR-AAM/67858/2006 and PTDC/AGR-AAM/102967/2008, as well as PostDoctoral Fellowships SFRH/BPD/44640/2008 and SFRH/BPD/81221/2011 awarded to E.R. and T.R.C., respectively).

AUTHOR CONTRIBUTIONS

E.R., P.B., M.C.T., J.F., I.S.-C. and P.D. designed the research, and E.R., T.R.C., P.B. and R.A.B. performed the experiments. E.R., T.R.C., P.B., R.A.B., M.C.T., J.F., I.S.-C. and P.D. analyzed the data, and the article was written by E.R. and P.D. with contributions from T.R.C., M.C.T. and I.S.-C.

FIGURE LEGENDS

Figure 1. *ZIFL1* Promoter Activity in *Arabidopsis*.

(A) to **(L)** Differential interference contrast microscopy images of GUS-stained transgenic plants carrying the *ProZIFL1:GUS* reporter construct. *ZIFL1* promoter activity in flowers **(A)**, a young leaf **(B)**, guard cells **(C)**, the shoot apical meristem **(D)**, the hypocotyl-root junction **(E)**, the primary root **(F)**, the primary root tip **(G)**, lateral root primordia at stage II **(H)**, stage V **(I)** and stage VII **(J)**, a newly emerged lateral root **(K)** and a mature lateral root tip **(L)**. Scale bars, 1 mm (A, B), 5 µm (C) or 50 µm (D-L). The arrowhead in (H) points to new cells emanating from the pericycle.

(M) to **(P)** Confocal laser scanning microscopy images of transgenic root tissues carrying the *ProZIFL1:GFP* reporter construct. *ZIFL1* promoter activity in the primary root **(M)**, the primary root tip **(N)** and a young **(O)** or mature **(P)** lateral root tip. Cell walls were stained with iodide propidium. The GFP and iodide propidium signals are visualized by green and red coloration, respectively. Scale bars, 50 µM.

Figure 2. Structure and Expression Pattern of the ZIFL1 Isoforms.

(A) Exon/intron organization of the *ZIFL1* gene and T-DNA insertion sites in the *zifl1-1* and *zifl1-2* mutants. Boxes and lines between boxes represent exons and introns, respectively. Triangles depict the sites of the T-DNA insertions. F1, F2, F3, F4, R1, R2 and R3 indicate the location of primers used to detect *ZIFL1* expression. The arrowhead points to the alternative 3' splice site. Scale bar, 100 bp.

(B) Structure of the alternative *ZIFL1* transcripts. Boxes indicate exons with UTRs in white, and lines between boxes represent introns. Transcript lengths are indicated. Scale bar, 100 nt.

(C) Predicted topology of the three putative ZIFL1 protein isoforms. Black boxes and curved lines denote membrane-spanning segments and hydrophilic regions, respectively. Predicted isoform sizes and molecular weights are indicated. Asterisks mark the position of the predicted protein truncation in the *zifl1-1* and *zifl1-2* mutants.

(D) RT-PCR profile of *ZIFL1* expression in different plant tissues. The location of the F1, F2 and R3 primers used is shown in (A). Expression of the *CYCLOPHILIN* (*ROC1*) gene was used as a loading control.

(E) RT-PCR analysis of *ZIFL1* expression in 14-d-old wild-type (Col-0) and mutant (*zifl1-1* and *zifl1-2)* seedlings. The location of the F1, F2, F3, F4, R1, R2 and R3 primers used is shown in (A). Expression of the *UBIQUITIN10* (*UBQ10*) gene was used as a loading

control.

Figure 3. Subcellular Localization of the ZIFL1 Isoforms.

(A) to **(C)** Confocal laser scanning microscopy images of *Arabidopsis* wild-type mesophyll protoplasts transiently expressing either YFP alone **(A)** or the ZIFL1.1-YFP **(B)** or ZIFL1.3-YFP **(C)** fusion proteins under the control of the 35S promoter. Arrowheads point to the YFP signal on the inner side of the chloroplasts and the nucleus. The YFP and chloroplast autofluorescence signals are visualized by green and red coloration, respectively.
(D) to **(F)** Confocal laser scanning microscopy images of an *Arabidopsis zifl1-2* mutant root tip **(D)** and a mature epidermal **(E)** or cortical **(F)** root cell stably expressing the ZIFL1.1-GFP fusion protein under the control of the endogenous *ZIFL1* promoter. The GFP and iodide propidium signals are visualized by green and red coloration, respectively. The arrowhead points to a transvacuolar strand. Scale bars, 50 µm (D) and 5 µm (E, F).
(G) to **(V)** Confocal laser scanning microscopy images of tobacco leaf epidermal cells transiently co-expressing the ZIFL1.1-GFP (**G** and **K**) or the ZIFL1.3-GFP (**O** and **S**) fusion proteins with the tonoplast marker γ-TIP-mCherry (**H** and **P**) or the plasma membrane marker PIP2A-mCherry (**L** and **T**) under the control of the 35S promoter. Merged images of whole-cell (**I**, **M**, **Q** and **U**) or close-up (**J**, **N**, **R** and **V**) views are shown. Arrowheads point to transvacuolar strands and asterisks indicate fluorescence signals approaching the nucleus only on the side facing the exterior of the cell. The GFP and mCherry signals are visualized by green and red coloration, respectively. Scale bars, 20 µm.

Figure 4. Drought-related Phenotypes of *ZIFL1* Loss-of-Function Mutants.

(A) Representative images of 5-week-old wild-type (Col-0) and *zifl1* mutant (*zifl1-1* and *zifl1-2*) plants grown under normal water supply (control conditions) or 7 d after terminating irrigation (drought stress).
(B) Water loss rates of rosette leaves detached from 5-week-old irrigated plants of the wild type (Col-0), the *zifl1* mutants (*zifl1-1* and *zifl1-2*) and two independent genomic complementation lines (*zifl1-1*comp and *zifl1-2*comp). Results are representative of three independent experiments and values represent means ± SD (n = 4).
(C) Stomatal apertures of rosette leaves detached from 5-week-old irrigated plants of the wild type (Col-0) and the *zifl1* mutants (*zifl1-1* and *zifl1-2*) after 3 h of light, dark or ABA (3

µM) treatment. Values represent the mean of four independent experiments ± SD. Asterisks denote statistically significant differences between *zifl1* mutants and the wild type (* $P<0.05$, ** $P<0.01$, *** $P<0.001$; Student's *t* test).

Figure 5. Auxin-related Phenotypes of *ZIFL1* Loss-of-Function Mutants.

(A) Representative images of 12-d-old wild-type (Col-0) and *zifl1* mutant (*zifl1-1* and *zifl1-2*) seedlings grown on control medium or medium supplemented with 0.025 µM 2,4-D or 0.05 µM IAA.

(B) Effect of 2,4-D (left panel) and IAA (right panel) on primary root elongation of 12-d-old seedlings of the wild type (Col-0), the *zifl1* mutants (*zifl1-1* and *zifl1-2*) and two independent genomic complementation lines (*zifl1-1*comp and *zifl1-2*comp). Results are representative of three independent experiments and values represent means ± SD (n = 16).

(C) Lateral root (LR) phenotype of 12-d-old seedlings of the wild type (Col-0), the *zifl1* mutants (*zifl1-1* and *zifl1-2*) and two independent genomic complementation lines (*zifl1-1*comp and *zifl1-2*comp). Total number of LRs (top panel), frequency of LR primordia (LRP) and emerged LRs (ELR) (middle panel) and LR length (lower panel) are presented. Results are representative of three independent experiments and bars represent means ± SD (n = 8).

(D) Root gravitropic response of 7-d-old seedlings of the wild type (Col-0), the *zifl1* mutants (*zifl1-1* and *zifl1-2*) and two independent genomic complementation lines (*zifl1-1*comp and *zifl1-2*comp) after 24 h of 90°-gravistimulation. The length of each bar represents the frequency of seedlings showing the direction of root tip curvature within the corresponding 30° sector. Results are representative of three independent experiments (n ≥ 30).

Asterisks denote statistically significant differences between *zifl1* mutants and the wild type (** $P<0.01$, *** $P<0.001$; Student's *t* test).

Figure 6. Phenotypes of Transgenic *Arabidopsis* Lines Overexpressing Individual ZIFL1 Isoforms.

(A) Effect of 2,4-D (left panel) and IAA (right panel) on primary root elongation of 12-d-old seedlings of the wild type (Col-0) and *ZIFL1*-overexpressing lines (*ZIFL1.1*OX, *ZIFL1.2*OX

and *ZIFL1.3*OX). Results are representative of three independent experiments and values represent means ± SD (*n* = 16).

(B) Lateral root (LR) phenotype of 12-d-old seedlings of the wild type (Col-0) and *ZIFL1*-overexpressing lines (*ZIFL1.1*OX, *ZIFL1.2*OX and *ZIFL1.3*OX). Total number of LRs (top panel), frequency of LR primordia (LRP) and emerged LRs (ELR) (middle panel) and LR length (lower panel) are presented. Results are representative of three independent experiments and bars represent means ± SD (*n* = 8).

(C) Root gravitropic response of 7-d-old seedlings of the wild type (Col-0) and *ZIFL1*-overexpressing lines (*ZIFL1.1*OX, *ZIFL1.2*OX and *ZIFL1.3*OX) after 6 h of 90°-gravistimulation. The length of each bar represents the frequency of seedlings showing the direction of root tip curvature within the corresponding 30° sector. Results are representative of three independent experiments (*n* ≥ 30).

(D) Water loss rates of rosette leaves detached from 5-week-old irrigated plants of the wild type (Col-0) and *ZIFL1*-overexpressing lines (*ZIFL1.1*OX, *ZIFL1.2*OX and *ZIFL1.3*OX). Results are representative of three independent experiments and values represent means ± SD (*n* = 4).

(E) Stomatal apertures of rosette leaves detached from 5-week-old irrigated plants of the wild type (Col-0) and *ZIFL1*-overexpressing lines (*ZIFL1.1*OX and *ZIFL1.3*OX) after 3 h of light, dark or ABA (3 µM) treatment. Values represent the mean of four independent experiments ± SD.

Asterisks denote statistically significant differences between *ZIFL1*-overexpressing lines and the wild type (** $P<0.01$, *** $P<0.001$; Student's *t* test).

Figure 7. ZIFL1.1 IAA Transport Activity in Yeast and *Arabidopsis*.

(A) Effect of the auxin polar efflux inhibitor NPA on [^{14}C]-IAA accumulation in non-adapted yeast *Δtpo1* mutant cells harboring either the cloning vector *pGREG576* or the *pGREG576_ZIFL1.1* or *pGREG576_ZIFL1.3* plasmids. Values represent the mean of four independent experiments ± SD.

(B) IAA efflux activity of root tips from wild-type (Col-0), *zifl1-1*-mutant and *ZIFL1.1*-overexpressing (*ZIFL1.1*OX) 5-d-old seedlings. Efflux is calculated as a percentage of the initial [^{14}C]-IAA loading. Results are representative of three independent experiments and bars represent means ± SD (*n* = 18).

(C) Representative differential interference contrast microscopy images of primary roots from wild-type (Col-0) and *zifl1*-mutant (*zifl1-1* and *zifl1-2*) 5-d-old seedlings expressing the auxin-responsive *ProDR5:GUS* construct. Seedlings were either not treated (Control) or treated with 1 µM IAA for 3 h at the hypocotyl-root junction (Rootward IAA) or at the root tip (Shootward IAA). Scale bars, 25 µm.

(D) Rootward and shootward IAA transport in primary roots from 5-d-old seedlings of the wild type (Col-0), the *eir1-4* and *zifl1-1* mutants, and the *ZIFL1.1*OX transgenic line in the absence (-NPA) or presence (+NPA) of 10 µM NPA. Values represent the mean of three independent experiments ± SD. For each genotype, the percentage of root IAA transport inhibition by NPA is indicated above the corresponding bars (P<0.01 for all genotypes in both polarities, except for shootward transport in *ZIFL1.1*OX where P<0.001).

Asterisks denote statistically significant differences between *zifl1* mutants or the *ZIFL1.1*OX line and the wild type (** P<0.01, *** P<0.001; Student's *t* test).

Figure 8. PIN2 Immunolocalization in *Arabidopsis zifl1-1* Mutant and *ZIFL1.1*-overexpressing Root Tips.

(A) Representative confocal laser scanning microscopy images of the PIN2 signal in root tips from 5-d-old wild-type (Col-0), *eir1-4* and *zifl1-1* mutant, and *ZIFL1.1*-overexpressing seedlings treated or not for 2 d with 0.1 µM IAA. Detection settings for staining visualization were identical for all genotypes. Arrowheads indicate the polarity of PIN2 localization. l, lateral root cap; c, cortex; e, epidermis. Signal intensities are coded blue to yellow corresponding to increasing intensity levels. Scale bars, 10 µm.

(B) Quantification of the PIN2 signal at the plasma membrane in root tip epidermal cells from seedlings of the wild type (Col-0), the *eir1-4* and *zifl1-1* mutants, and the *ZIFL1.1*OX transgenic line. Average fluorescence (pixel) intensity values represent the mean of three independent experiments ± SD (n > 24). Asterisks denote statistically significant differences from the wild type under each condition (* P<0.05, *** P<0.001; Student's *t* test).

Figure 9. Potassium and Proton Transport Activity of ZIFL1.1 and ZIFL1.3 in Yeast and *Arabidopsis*.

(A) Susceptibility to low potassium growth conditions of yeast *Δqdr2* mutant cells harboring

either the cloning vector *pGREG576* or the *pGREG576_ZIFL1.1* or *pGREG576_ZIFL1.3* plasmids determined by spotting dilution series of cell suspensions (1, 1:5, and 1:10).

(B) Effect of K^+ and Cs^+ on primary root elongation of 12-d-old seedlings of the wild type (Col-0), the *zifl1* mutants (*zifl1-1* and *zifl1-2*) and the *ZIFL1.1*OX transgenic line. Results are representative of three independent experiments and bars represent means ± SD (*n* = 16). Asterisks denote statistically significant differences between *zifl1* mutants or the *ZIFL1.1*OX line and the wild type (*** *P*<0.001; Student's *t* test).

(C) Lateral root (LR) phenotype of 12-d-old seedlings of the wild type (Col-0), the *zifl1* mutants (*zifl1-1* and *zifl1-2*) and the *ZIFL1.1*OX line in the presence of 2 mM Cs^+. Total number of LRs (top panel), frequency of LR primordia (LRP) and emerged LRs (ELR) (middle panel) and LR length (lower panel) are presented. Results are representative of three independent experiments and bars represent means ± SD (*n* = 8).

(D) External medium acidification promoted by energized yeast *Δqdr2* mutant cells harboring either the cloning vector *pGREG576* or the *pGREG576_ZIFL1.1* or *pGREG576_ZIFL1.3* plasmids. Results are representative of three independent experiments.

(E) Confocal laser scanning microscopy images of *Arabidopsis* root tip epidermal cells of 5-d-old wild-type, *zifl1-1*-mutant and *ZIFL1.1*-overexpressing seedlings stained with acridine orange. Detection settings for staining visualization were identical for all genotypes, and numbers below each image indicate the average fluorescence (pixel) intensity representative of one of three independent experiments (means ± SD, *n* = 8). Scale bars, 25 μm.

Table 1. Complementation of *zifl1* Mutant Phenotypes by the ZIFL1.1 and ZIFL1.3 Isoforms.

	Primary root elongation (cm)[a]			Water loss (% FW)[b]
	Control	**0.025 µM 2,4-D**	**0.05 µM IAA**	
Col-0	4.56 ± 0.46	2.93 ± 0.33	3.98 ± 0.66	20.53 ± 1.65
zifl1-1	4.63 ± 0.53	2.41 ± 0.26 ($1.8e^{-5}$)	3.05 ± 0.42 ($3.7e^{-5}$)	35.86 ± 1.53 ($1.12e^{-5}$)
zifl1-2	4.57 ± 0.69	2.38 ± 0.47 ($3.9e^{-4}$)	2.95 ± 0.64 ($8.2e^{-5}$)	36.44 ± 4.44 ($5.6e^{-4}$)
zifl1-1*/Pro*ZIFL1*:*ZIFL1.1-GFP	4.39 ± 0.68	2.77 ± 0.62 (0.20)	3.65 ± 0.65 (0.10)	34.73 ± 1.67 ($2.2e^{-5}$)
zifl1-1*/Pro*ZIFL1*:*ZIFL1.3-GFP	4.49 ± 0.41	2.46 ± 0.37 ($4.2e^{-4}$)	2.97 ± 0.47 ($1.9e^{-5}$)	20.89 ± 3.79 (0.44)
zifl1-2*/Pro*ZIFL1*:*ZIFL1.1-GFP	4.34 ± 0.46	2.76 ± 0.33 (0.09)	3.82 ± 0.32 (0.21)	36.24 ± 2.29 ($3.6e^{-5}$)
zifl1-2*/Pro*ZIFL1*:*ZIFL1.3-GFP	4.42 ± 0.39	2.39 ± 0.41 ($1.7e^{-4}$)	2.80 ± 0.43 ($1.3e^{-6}$)	21.32 ± 3.15 (0.36)

[a] Effect of 2,4-D and IAA on primary root elongation of 12-d-old seedlings of the wild type (Col-0), the *zifl1* mutants (*zifl1-1* and *zifl1-2*) and two independent mutant lines complemented with either the Pro*ZIFL1*:*ZIFL1.1-GFP or* Pro*ZIFL1*:*ZIFL1.3-GFP* constructs. Results are representative of three independent experiments and values represent means ± SD (n = 16).

[b] Water loss rates of 5-week-old irrigated plants of the wild type (Col-0), the *zifl1* mutants (*zifl1-1* and *zifl1-2*) and two independent mutant lines complemented with either Pro*ZIFL1*:*ZIFL1.1-GFP or* Pro*ZIFL1*:*ZIFL1.3-GFP*. Results are representative of three independent experiments and values represent means ± SD (n = 4).

Numbers between parentheses indicate the P values (wild type versus *zifl1* mutants or *ZIFL1* transgenic lines) obtained by Student's t test.

Table 2. Accumulation of Radiolabeled Auxins in Yeast and *Arabidopsis*.

	Relative auxin accumulation		
	2,4-D	**IAA**	**NAA**
Yeast[a]			
Δ*tpo1* + *pGREG576*	13.97 ± 1.29	28.70 ± 2.08	*ND*
Δ*tpo1* + GFP-ZIFL1.1	7.26 ± 0.89 ($1.2e^{-6}$)	12.96 ± 2.36 ($2.1e^{-7}$)	*ND*
Δ*tpo1* + GFP-ZIFL1.3	7.40 ± 0.64 ($6.7e^{-7}$)	15.03 ± 1.70 ($2.4e^{-7}$)	*ND*
Arabidopsis[b]			
Col-0	100.00 ± 11.64	100.00 ± 11.99	100.00 ± 14.38
zifl1-1	141.70 ± 10.40 ($3.8e^{-11}$)	120.52 ± 9.26 ($1.6e^{-6}$)	103.94 ± 14.91 (0.22)
zifl1-2	134.88 ± 19.89 ($6.5e^{-6}$)	121.83 ± 12.41 ($1.4e^{-5}$)	106.19 ± 16.16 (0.13)
***ZIFL1.1*OX**	77.38 ± 8.43 ($1.2e^{-7}$)	85.71 ± 9.19 ($1.3e^{-4}$)	99.53 ± 9.87 (0.45)
***ZIFL1.3*OX**	96.74 ± 16.00 (0.27)	95.24 ± 11.74 (0.12)	106.98 ± 17.67 (0.11)

[a] Accumulation ratio (intra/extracellular) of [^{14}C]-2,4-D or [^{14}C]-IAA in non-adapted yeast *Δtpo1* mutant cells harboring either the cloning vector *pGREG576* or the *pGREG576_ZIFL1.1* or *pGREG576_ZIFL1.3* plasmids. Results are from three independent experiments and values represent means ± SD (*n* = 6).

[b] Relative [^{14}C]-2,4-D, [^{14}C]-IAA or [^{14}C]-NAA accumulation in root tips from 5-d-old seedlings of the wild type (Col-0), the *zifl1* mutants (*zifl1-1* and *zifl1-2*) and the *ZIFL1.1*OX or *ZIFL1.3*OX transgenic lines. Data are expressed relative to wild-type accumulation. Results are from three independent experiments and values represent means ± SD (*n* = 12).

Numbers between parentheses indicate the *P* values (yeast Δ*tpo1* mutant versus *ZIFL1.1* or *ZIFL1.3*-expressing Δ*tpo1* lines, or *Arabidopsis* wild type versus *zifl1* mutants or *ZIFL1*-overexpressing lines) obtained by Student's *t* test.

ND, not determined.

Table 3. Effect of Polar Auxin Transport Inhibitors on Wild-type, *zifl1*-Mutant and *ZIFL1*-overexpressing Seedlings.

	Relative primary root elongation (%)[a]			
	Control	**10 µM NOA**	**10 µM NPA**	**1 µM TIBA**
Col-0	100.00 ± 5.89	76.06 ± 6.27	38.09 ± 9.84	75.67 ± 9.91
zifl1-1	100.00 ± 4.76	74.28 ± 8.18 (0.26)	59.00 ± 6.57 ($6.0e^{-8}$)	90.19 ± 9.82 ($1.7e^{-4}$)
zifl1-2	100.00 ± 6.79	73.02 ± 6.36 (0.10)	55.02 ± 9.98 ($2.6e^{-5}$)	87.65 ± 4.82 ($1.1e^{-4}$)
***ZIFL1.1*OX**	100.00 ± 3.60	73.40 ± 6.97 (0.15)	24.08 ± 3.60 ($7.5e^{-6}$)	57.15 ± 7.55 ($1.3e^{-6}$)
***ZIFL1.3*OX**	100.00 ± 6.06	74.53 ± 6.90 (0.27)	38.04 ± 6.43 (0.49)	78.49 ± 8.63 (0.21)

[a] Effect of the auxin polar transport inhibitors NOA, NPA and TIBA on primary root elongation of 12-d-old seedlings of the wild-type (Col-0), the *zifl1* mutants (*zifl1-1* and *zifl1-2*) and the *ZIFL1.1*OX or *ZIFL1.3*OX transgenic lines. Results are representative of three independent experiments and values represent means ± SD (n = 16).
Numbers between parentheses indicate the P values (wild type versus *zifl1* mutants or *ZIFL1*-overexpressing lines) obtained by Student's t test.

REFERENCES

Abas, L., Benjamins, R., Malenica, N., Paciorek, T., Wisniewska, J., Moulinier-Anzola, J.C., Sieberer, T., Friml, J., and Luschnig, C. (2006). Intracellular trafficking and proteolysis of the Arabidopsis auxin-efflux facilitator PIN2 are involved in root gravitropism. Nat Cell Biol **8,** 249-256.

Abel, S., and Theologis, A. (1994). Transient transformation of Arabidopsis leaf protoplasts: a versatile experimental system to study gene expression. Plant J **5,** 421-427.

Araújo, W.L., Fernie, A.R., and Nunes-Nesi, A. (2011). Control of stomatal aperture: a renaissance of the old guard. Plant Signal Behav **6,** 1305-1311.

Bassham, D.C., and Raikhel, N.V. (2000). Plant cells are not just green yeast. Plant Physiol **122,** 999-1001.

Baster, P., Robert, S., Kleine-Vehn, J., Vanneste, S., Kania, U., Grunewald, W., De Rybel, B., Beeckman, T., and Friml, J. (2012). SCF(TIR1/AFB)-auxin signalling regulates PIN vacuolar trafficking and auxin fluxes during root gravitropism. EMBO J **32,** 260-274.

Bennett, M.J., Marchant, A., Green, H.G., May, S.T., Ward, S.P., Millner, P.A., Walker, A.R., Schulz, B., and Feldmann, K.A. (1996). Arabidopsis AUX1 gene: a permease-like regulator of root gravitropism. Science **273,** 948-950.

Blakeslee, J.J., Bandyopadhyay, A., Lee, O.R., Mravec, J., Titapiwatanakun, B., Sauer, M., Makam, S.N., Cheng, Y., Bouchard, R., Adamec, J., Geisler, M., Nagashima, A., Sakai, T., Martinoia, E., Friml, J., Peer, W.A., and Murphy, A.S. (2007). Interactions among PIN-FORMED and P-glycoprotein auxin transporters in Arabidopsis. Plant Cell **19,** 131-147.

Blilou, I., Xu, J., Wildwater, M., Willemsen, V., Paponov, I., Friml, J., Heidstra, R., Aida, M., Palme, K., and Scheres, B. (2005). The PIN auxin efflux facilitator network controls growth and patterning in Arabidopsis roots. Nature **433,** 39-44.

Boonsirichai, K., Sedbrook, J.C., Chen, R., Gilroy, S., and Masson, P.H. (2003). ALTERED RESPONSE TO GRAVITY is a peripheral membrane protein that modulates gravity-induced cytoplasmic alkalinization and lateral auxin transport in plant statocytes. Plant Cell **15,** 2612-2625.

Bright, J., Desikan, R., Hancock, J.T., Weir, I.S., and Neill, S.J. (2006). ABA-induced NO generation and stomatal closure in Arabidopsis are dependent on H2O2 synthesis. Plant J **45,** 113-122.

Buttner, M. (2007). The monosaccharide transporter(-like) gene family in Arabidopsis. FEBS Lett **581,** 2318-2324.

Cabrito, T.R., Teixeira, M.C., Duarte, A.A., Duque, P., and Sá-Correia, I. (2009). Heterologous expression of a Tpo1 homolog from Arabidopsis thaliana confers resistance to the herbicide 2,4-D and other chemical stresses in yeast. Appl Microbiol Biotechnol **84,** 927-936.

Chen, R., Hilson, P., Sedbrook, J., Rosen, E., Caspar, T., and Masson, P.H. (1998). The arabidopsis thaliana AGRAVITROPIC 1 gene encodes a component of the polar-auxin-transport efflux carrier. Proc Natl Acad Sci U S A **95,** 15112-15117.

Christian, M., Steffens, B., Schenck, D., Burmester, S., Bottger, M., and Luthen, H. (2006). How does auxin enhance cell elongation? Roles of auxin-binding proteins and potassium channels in growth control. Plant Biol (Stuttg) **8,** 346-352.

Clough, S.J., and Bent, A.F. (1998). Floral dip: a simplified method for Agrobacterium-mediated transformation of Arabidopsis thaliana. Plant J **16,** 735-743.

Delbarre, A., Muller, P., Imhoff, V., and Guern, J. (1996). Comparison of mechanisms controlling uptake and accumulation of 2,4-dichlorophenoxy acetic acid, naphthalene-1-acetic acid, and indole-3-acetic acid in suspension-cultured tobacco cells. Planta **198,** 532-541.

Delker, C., Poschl, Y., Raschke, A., Ullrich, K., Ettingshausen, S., Hauptmann, V., Grosse, I., and Quint, M. (2010). Natural variation of transcriptional auxin response networks in Arabidopsis thaliana. Plant Cell **22,** 2184-2200.

Dhonukshe, P., Aniento, F., Hwang, I., Robinson, D.G., Mravec, J., Stierhof, Y.D., and Friml, J. (2007). Clathrin-mediated constitutive endocytosis of PIN auxin efflux carriers in Arabidopsis. Curr Biol **17,** 520-527.

Earley, K.W., Haag, J.R., Pontes, O., Opper, K., Juehne, T., Song, K., and Pikaard, C.S. (2006). Gateway-compatible vectors for plant functional genomics and proteomics. Plant J **45,** 616-629.

Friml, J., Wisniewska, J., Benkova, E., Mendgen, K., and Palme, K. (2002). Lateral relocation of auxin efflux regulator PIN3 mediates tropism in Arabidopsis. Nature **415,** 806-809.

Fuchs, I., Philippar, K., and Hedrich, R. (2006). Ion channels meet auxin action. Plant Biol (Stuttg) **8,** 353-359.

Gaedeke, N., Klein, M., Kolukisaoglu, U., Forestier, C., Muller, A., Ansorge, M., Becker, D., Mamnun, Y., Kuchler, K., Schulz, B., Mueller-Roeber, B., and Martinoia, E. (2001). The Arabidopsis thaliana ABC transporter AtMRP5 controls root development and stomata movement. EMBO J **20,** 1875-1887.

Geisler, M., Blakeslee, J.J., Bouchard, R., Lee, O.R., Vincenzetti, V., Bandyopadhyay, A., Titapiwatanakun, B., Peer, W.A., Bailly, A., Richards, E.L., Ejendal, K.F., Smith, A.P., Baroux, C., Grossniklaus, U., Muller, A., Hrycyna, C.A., Dudler, R., Murphy, A.S., and Martinoia, E. (2005). Cellular efflux of auxin catalyzed by the Arabidopsis MDR/PGP transporter AtPGP1. Plant J **44,** 179-194.

Geldner, N., Friml, J., Stierhof, Y.D., Jurgens, G., and Palme, K. (2001). Auxin transport inhibitors block PIN1 cycling and vesicle trafficking. Nature **413,** 425-428.

Goldsmith, M.H.M. (1977). Polar transport of auxin. Annual Review Plant Physiology Plant Molecular Biology, 439-478.

Hampton, C.R., Bowen, H.C., Broadley, M.R., Hammond, J.P., Mead, A., Payne, K.A., Pritchard, J., and White, P.J. (2004). Cesium toxicity in Arabidopsis. Plant Physiol **136,** 3824-3837.

Haydon, M.J., and Cobbett, C.S. (2007). A novel major facilitator superfamily protein at the tonoplast influences zinc tolerance and accumulation in Arabidopsis. Plant Physiol **143,** 1705-1719.

Hirano, T., Matsuzawa, T., Takegawa, K., and Sato, M.H. (2011). Loss-of-function and gain-of-function mutations in FAB1A/B impair endomembrane homeostasis, conferring pleiotropic developmental abnormalities in Arabidopsis. Plant Physiol **155,** 797-807.

Huala, E., Dickerman, A.W., Garcia-Hernandez, M., Weems, D., Reiser, L., LaFond, F., Hanley, D., Kiphart, D., Zhuang, M., Huang, W., Mueller, L.A., Bhattacharyya, D., Bhaya, D., Sobral, B.W., Beavis, W., Meinke, D.W., Town, C.D., Somerville, C., and Rhee, S.Y. (2001). The Arabidopsis Information Resource (TAIR): a

comprehensive database and web-based information retrieval, analysis, and visualization system for a model plant. Nucleic Acids Res **29,** 102-105.

Ito, H., and Gray, W.M. (2006). A gain-of-function mutation in the Arabidopsis pleiotropic drug resistance transporter PDR9 confers resistance to auxinic herbicides. Plant Physiol **142,** 63-74.

Jansen, G., Wu, C., Schade, B., Thomas, D.Y., and Whiteway, M. (2005). Drag&Drop cloning in yeast. Gene **344,** 43-51.

Karimi, M., Inze, D., and Depicker, A. (2002). GATEWAY vectors for Agrobacterium-mediated plant transformation. Trends Plant Sci **7,** 193-195.

Kleine-Vehn, J., Dhonukshe, P., Swarup, R., Bennett, M., and Friml, J. (2006). Subcellular trafficking of the Arabidopsis auxin influx carrier AUX1 uses a novel pathway distinct from PIN1. Plant Cell **18,** 3171-3181.

Kleine-Vehn, J., Leitner, J., Zwiewka, M., Sauer, M., Abas, L., Luschnig, C., and Friml, J. (2008a). Differential degradation of PIN2 auxin efflux carrier by retromer-dependent vacuolar targeting. Proc Natl Acad Sci U S A **105,** 17812-17817.

Kleine-Vehn, J., Dhonukshe, P., Sauer, M., Brewer, P.B., Wisniewska, J., Paciorek, T., Benkova, E., and Friml, J. (2008b). ARF GEF-dependent transcytosis and polar delivery of PIN auxin carriers in Arabidopsis. Curr Biol **18,** 526-531.

Krouk, G., Lacombe, B., Bielach, A., Perrine-Walker, F., Malinska, K., Mounier, E., Hoyerova, K., Tillard, P., Leon, S., Ljung, K., Zazimalova, E., Benkova, E., Nacry, P., and Gojon, A. (2010). Nitrate-regulated auxin transport by NRT1.1 defines a mechanism for nutrient sensing in plants. Dev Cell **18,** 927-937.

Laxmi, A., Pan, J., Morsy, M., and Chen, R. (2008). Light plays an essential role in intracellular distribution of auxin efflux carrier PIN2 in Arabidopsis thaliana. PLoS One **3,** e1510.

Lewis, D.R., and Muday, G.K. (2009). Measurement of auxin transport in Arabidopsis thaliana. Nat Protoc **4,** 437-451.

Lewis, D.R., Miller, N.D., Splitt, B.L., Wu, G., and Spalding, E.P. (2007). Separating the roles of acropetal and basipetal auxin transport on gravitropism with mutations in two Arabidopsis multidrug resistance-like ABC transporter genes. Plant Cell **19,** 1838-1850.

Li, J., Yang, H., Peer, W.A., Richter, G., Blakeslee, J., Bandyopadhyay, A., Titapiwantakun, B., Undurraga, S., Khodakovskaya, M., Richards, E.L., Krizek, B., Murphy, A.S., Gilroy, S., and Gaxiola, R. (2005). Arabidopsis H+-PPase AVP1 regulates auxin-mediated organ development. Science **310,** 121-125.

Li, P., Sioson, A., Mane, S.P., Ulanov, A., Grothaus, G., Heath, L.S., Murali, T.M., Bohnert, H.J., and Grene, R. (2006). Response diversity of Arabidopsis thaliana ecotypes in elevated [CO2] in the field. Plant Mol Biol **62,** 593-609.

Lin, R., and Wang, H. (2005). Two homologous ATP-binding cassette transporter proteins, AtMDR1 and AtPGP1, regulate Arabidopsis photomorphogenesis and root development by mediating polar auxin transport. Plant Physiol **138,** 949-964.

Löfke, C., Luschnig, C., and Kleine-Vehn, J. (2013). Posttranslational modification and trafficking of PIN auxin efflux carriers. Mech Dev **130,** 82-94.

Luschnig, C., Gaxiola, R.A., Grisafi, P., and Fink, G.R. (1998). EIR1, a root-specific protein involved in auxin transport, is required for gravitropism in Arabidopsis thaliana. Genes Dev **12,** 2175-2187.

Malamy, J.E., and Benfey, P.N. (1997). Organization and cell differentiation in lateral roots of Arabidopsis thaliana. Development **124,** 33-44.

Malenica, N., Abas, L., Benjamins, R., Kitakura, S., Sigmund, H.F., Jun, K.S., Hauser, M.T., Friml, J., and Luschnig, C. (2007). MODULATOR OF PIN genes control steady-state levels of Arabidopsis PIN proteins. Plant J **51,** 537-550.

Marchant, A., Kargul, J., May, S.T., Muller, P., Delbarre, A., Perrot-Rechenmann, C., and Bennett, M.J. (1999). AUX1 regulates root gravitropism in Arabidopsis by facilitating auxin uptake within root apical tissues. EMBO J **18,** 2066-2073.

Marquez, Y., Brown, J.W., Simpson, C., Barta, A., and Kalyna, M. (2012). Transcriptome survey reveals increased complexity of the alternative splicing landscape in Arabidopsis. Genome Res **22,** 1184-1195.

Meyer, S., Mumm, P., Imes, D., Endler, A., Weder, B., Al-Rasheid, K.A., Geiger, D., Marten, I., Martinoia, E., and Hedrich, R. (2010). AtALMT12 represents an R-type anion channel required for stomatal movement in Arabidopsis guard cells. Plant J **63,** 1054-1062.

Mitchell, E.K., and Davies, P.J. (1975). Evidence for 3 Different Systems of Movement of Indoleacetic-Acid in Intact Roots of Phaseolus-Coccineus. Physiologia Plantarum **33,** 290-294.

Mittelheuser, C.J., and Van Steveninck, R.F.M. (1969). Stomatal Closure and Inhibition of Transpiration Induced by (Rs)-Abscisic Acid. Nature **221,** 281-&.

Mravec, J., Kubes, M., Bielach, A., Gaykova, V., Petrasek, J., Skupa, P., Chand, S., Benkova, E., Zazimalova, E., and Friml, J. (2008). Interaction of PIN and PGP transport mechanisms in auxin distribution-dependent development. Development **135,** 3345-3354.

Müller, A., Guan, C., Gälweiler, L., Tänzler, P., Huijser, P., Marchant, A., Parry, G., Bennett, M., Wisman, E., and Palme, K. (1998). AtPIN2 defines a locus of Arabidopsis for root gravitropism control. EMBO J **17,** 6903-6911.

Munos, S., Cazettes, C., Fizames, C., Gaymard, F., Tillard, P., Lepetit, M., Lejay, L., and Gojon, A. (2004). Transcript profiling in the chl1-5 mutant of Arabidopsis reveals a role of the nitrate transporter NRT1.1 in the regulation of another nitrate transporter, NRT2.1. Plant Cell **16,** 2433-2447.

Murashige, T., and Skoog, F. (1962). A revised medium for rapid growth and bioassays with tobacco tissue culture. Physiol Plant **15,** 473-497.

Murphy, A.S., Hoogner, K.R., Peer, W.A., and Taiz, L. (2002). Identification, purification, and molecular cloning of N-1-naphthylphthalmic acid-binding plasma membrane-associated aminopeptidases from Arabidopsis. Plant Physiol **128,** 935-950.

Nagy, R., Grob, H., Weder, B., Green, P., Klein, M., Frelet-Barrand, A., Schjoerring, J.K., Brearley, C., and Martinoia, E. (2009). The Arabidopsis ATP-binding cassette protein AtMRP5/AtABCC5 is a high affinity inositol hexakisphosphate transporter involved in guard cell signaling and phytate storage. J Biol Chem **284,** 33614-33622.

Noh, B., Murphy, A.S., and Spalding, E.P. (2001). Multidrug resistance-like genes of Arabidopsis required for auxin transport and auxin-mediated development. Plant Cell **13,** 2441-2454.

Okada, K., Ueda, J., Komaki, M.K., Bell, C.J., and Shimura, Y. (1991). Requirement of the Auxin Polar Transport System in Early Stages of Arabidopsis Floral Bud Formation. Plant Cell **3,** 677-684.

Paciorek, T., and Friml, J. (2006). Auxin signaling. J Cell Sci **119,** 1199-1202.

Paciorek, T., Zazimalova, E., Ruthardt, N., Petrasek, J., Stierhof, Y.D., Kleine-Vehn, J., Morris, D.A., Emans, N., Jurgens, G., Geldner, N., and Friml, J. (2005). Auxin inhibits endocytosis and promotes its own efflux from cells. Nature **435,** 1251-1256.

Pao, S.S., Paulsen, I.T., and Saier, M.H., Jr. (1998). Major facilitator superfamily. Microbiol Mol Biol Rev **62,** 1-34.

Park, S., Li, J., Pittman, J.K., Berkowitz, G.A., Yang, H., Undurraga, S., Morris, J., Hirschi, K.D., and Gaxiola, R.A. (2005). Up-regulation of a H+-pyrophosphatase (H+-PPase) as a strategy to engineer drought-resistant crop plants. Proc Natl Acad Sci U S A **102,** 18830-18835.

Peer, W.A., Bandyopadhyay, A., Blakeslee, J.J., Makam, S.N., Chen, R.J., Masson, P.H., and Murphy, A.S. (2004). Variation in expression and protein localization of the PIN family of auxin efflux facilitator proteins in flavonoid mutants with altered auxin transport in Arabidopsis thaliana. Plant Cell **16,** 1898-1911.

Petrasek, J., and Friml, J. (2009). Auxin transport routes in plant development. Development **136,** 2675-2688.

Petrasek, J., Mravec, J., Bouchard, R., Blakeslee, J.J., Abas, M., Seifertova, D., Wisniewska, J., Tadele, Z., Kubes, M., Covanova, M., Dhonukshe, P., Skupa, P., Benkova, E., Perry, L., Krecek, P., Lee, O.R., Fink, G.R., Geisler, M., Murphy, A.S., Luschnig, C., Zazimalova, E., and Friml, J. (2006). PIN proteins perform a rate-limiting function in cellular auxin efflux. Science **312,** 914-918.

Qi, Z., Hampton, C.R., Shin, R., Barkla, B.J., White, P.J., and Schachtman, D.P. (2008). The high affinity K+ transporter AtHAK5 plays a physiological role in planta at very low K+ concentrations and provides a caesium uptake pathway in Arabidopsis. J Exp Bot **59,** 595-607.

Rahman, A., Bannigan, A., Sulaman, W., Pechter, P., Blancaflor, E.B., and Baskin, T.I. (2007). Auxin, actin and growth of the Arabidopsis thaliana primary root. Plant J **50,** 514-528.

Rahman, A., Takahashi, M., Shibasaki, K., Wu, S., Inaba, T., Tsurumi, S., and Baskin, T.I. (2010). Gravitropism of Arabidopsis thaliana roots requires the polarization of PIN2 toward the root tip in meristematic cortical cells. Plant Cell **22,** 1762-1776.

Rashotte, A.M., Poupart, J., Waddell, C.S., and Muday, G.K. (2003). Transport of the two natural auxins, indole-3-butyric acid and indole-3-acetic acid, in Arabidopsis. Plant Physiol **133,** 761-772.

Rashotte, A.M., Brady, S.R., Reed, R.C., Ante, S.J., and Muday, G.K. (2000). Basipetal auxin transport is required for gravitropism in roots of Arabidopsis. Plant Physiol **122,** 481-490.

Raven, J.A. (1975). Transport of indoleacetic acid in plant-cells in relation to pH and electrical potencial gradients, and its significance to polar IAA transport. New Phytologist **4,** 163-172.

Rea, P.A. (2007). Plant ATP-binding cassette transporters. Annu Rev Plant Biol **58,** 347-375.

Reinhardt, D., Pesce, E.R., Stieger, P., Mandel, T., Baltensperger, K., Bennett, M., Traas, J., Friml, J., and Kuhlemeier, C. (2003). Regulation of phyllotaxis by polar auxin transport. Nature **426,** 255-260.

Remy, E., Cabrito, T.R., Batista, R.A., Teixeira, M.C., Sa-Correia, I., and Duque, P. (2012). The Pht1;9 and Pht1;8 transporters mediate inorganic phosphate acquisition by the Arabidopsis thaliana root during phosphorus starvation. New Phytol **195,** 356-371.

Ren, Q., Kang, K.H., and Paulsen, I.T. (2004). TransportDB: a relational database of cellular membrane transport systems. Nucleic Acids Res **32,** D284-288.

Rubery, P.H., and Sheldrake, A.R. (1974). Carrier-mediated auxin transport. Planta **118,** 101-121.

Sabatini, S., Beis, D., Wolkenfelt, H., Murfett, J., Guilfoyle, T., Malamy, J., Benfey, P., Leyser, O., Bechtold, N., Weisbeek, P., and Scheres, B. (1999). An auxin-dependent distal organizer of pattern and polarity in the Arabidopsis root. Cell **99,** 463-472.

Santelia, D., Vincenzetti, V., Azzarello, E., Bovet, L., Fukao, Y., Duchtig, P., Mancuso, S., Martinoia, E., and Geisler, M. (2005). MDR-like ABC transporter AtPGP4 is involved in auxin-mediated lateral root and root hair development. FEBS Lett **579,** 5399-5406.

Sauer, M., Paciorek, T., Benkova, E., and Friml, J. (2006). Immunocytochemical techniques for whole-mount in situ protein localization in plants. Nat Protoc **1,** 98-103.

Serrano, R. (1978). Characterization of the plasma membrane ATPase of Saccharomyces cerevisiae. Mol Cell Biochem **22,** 51-63.

Shin, H., Shin, H.S., Dewbre, G.R., and Harrison, M.J. (2004). Phosphate transport in Arabidopsis: Pht1;1 and Pht1;4 play a major role in phosphate acquisition from both low- and high-phosphate environments. Plant J **39,** 629-642.

Sieberer, T., Seifert, G.J., Hauser, M.T., Grisafi, P., Fink, G.R., and Luschnig, C. (2000). Post-transcriptional control of the Arabidopsis auxin efflux carrier EIR1 requires AXR1. Curr Biol **10,** 1595-1598.

Suh, S.J., Wang, Y.F., Frelet, A., Leonhardt, N., Klein, M., Forestier, C., Mueller-Roeber, B., Cho, M.H., Martinoia, E., and Schroeder, J.I. (2007). The ATP binding cassette transporter AtMRP5 modulates anion and calcium channel activities in Arabidopsis guard cells. J Biol Chem **282,** 1916-1924.

Sundaresan, V., Springer, P., Volpe, T., Haward, S., Jones, J.D., Dean, C., Ma, H., and Martienssen, R. (1995). Patterns of gene action in plant development revealed by enhancer trap and gene trap transposable elements. Genes Dev **9,** 1797-1810.

Swarup, K., Benkova, E., Swarup, R., Casimiro, I., Peret, B., Yang, Y., Parry, G., Nielsen, E., De Smet, I., Vanneste, S., Levesque, M.P., Carrier, D., James, N., Calvo, V., Ljung, K., Kramer, E., Roberts, R., Graham, N., Marillonnet, S., Patel, K., Jones, J.D., Taylor, C.G., Schachtman, D.P., May, S., Sandberg, G., Benfey, P., Friml, J., Kerr, I., Beeckman, T., Laplaze, L., and Bennett, M.J. (2008). The auxin influx carrier LAX3 promotes lateral root emergence. Nat Cell Biol **10,** 946-954.

Swarup, R., Friml, J., Marchant, A., Ljung, K., Sandberg, G., Palme, K., and Bennett, M. (2001). Localization of the auxin permease AUX1 suggests two functionally distinct hormone transport pathways operate in the Arabidopsis root apex. Genes Dev **15,** 2648-2653.

Tanaka, H., Dhonukshe, P., Brewer, P.B., and Friml, J. (2006). Spatiotemporal asymmetric auxin distribution: a means to coordinate plant development. Cell Mol Life Sci **63,** 2738-2754.

Teixeira, M.C., and Sá-Correia, I. (2002). Saccharomyces cerevisiae resistance to chlorinated phenoxyacetic acid herbicides involves Pdr1p-mediated transcriptional activation of TPO1 and PDR5 genes. Biochem Biophys Res Commun **292,** 530-537.

Terasaka, K., Blakeslee, J.J., Titapiwatanakun, B., Peer, W.A., Bandyopadhyay, A., Makam, S.N., Lee, O.R., Richards, E.L., Murphy, A.S., Sato, F., and Yazaki, K. (2005). PGP4, an ATP binding cassette P-glycoprotein, catalyzes auxin transport in Arabidopsis thaliana roots. Plant Cell **17,** 2922-2939.

Thimann, K.V., and Satler, S.O. (1979). Relation between leaf senescence and stomatal closure: Senescence in light. Proc Natl Acad Sci U S A **76,** 2295-2298.

Titapiwatanakun, B., Blakeslee, J.J., Bandyopadhyay, A., Yang, H., Mravec, J., Sauer, M., Cheng, Y., Adamec, J., Nagashima, A., Geisler, M., Sakai, T., Friml, J., Peer, W.A., and Murphy, A.S. (2009). ABCB19/PGP19 stabilises PIN1 in membrane microdomains in Arabidopsis. Plant J **57,** 27-44.

Tsay, Y.F., Chiu, C.C., Tsai, C.B., Ho, C.H., and Hsu, P.K. (2007). Nitrate transporters and peptide transporters. FEBS Lett **581,** 2290-2300.

Tsurumi, S., and Ohwaki, Y. (1978). Transport of C-14-Labeled Indoleacetic-Acid in Vicia Root Segments. Plant and Cell Physiology **19,** 1195-1206.

Ulmasov, T., Murfett, J., Hagen, G., and Guilfoyle, T.J. (1997). Aux/IAA proteins repress expression of reporter genes containing natural and highly active synthetic auxin response elements. Plant Cell **9,** 1963-1971.

Vargas, R.C., Garcia-Salcedo, R., Tenreiro, S., Teixeira, M.C., Fernandes, A.R., Ramos, J., and Sá-Correia, I. (2007). Saccharomyces cerevisiae multidrug resistance transporter Qdr2 is implicated in potassium uptake, providing a physiological advantage to quinidine-stressed cells. Eukaryot Cell **6,** 134-142.

Vicente-Agullo, F., Rigas, S., Desbrosses, G., Dolan, L., Hatzopoulos, P., and Grabov, A. (2004). Potassium carrier TRH1 is required for auxin transport in Arabidopsis roots. Plant J **40,** 523-535.

Vieten, A., Sauer, M., Brewer, P.B., and Friml, J. (2007). Molecular and cellular aspects of auxin-transport-mediated development. Trends Plant Sci **12,** 160-168.

Vieten, A., Vanneste, S., Wisniewska, J., Benkova, E., Benjamins, R., Beeckman, T., Luschnig, C., and Friml, J. (2005). Functional redundancy of PIN proteins is

accompanied by auxin-dependent cross-regulation of PIN expression. Development **132,** 4521-4531.

Voinnet, O., Rivas, S., Mestre, P., and Baulcombe, D. (2003). An enhanced transient expression system in plants based on suppression of gene silencing by the p19 protein of tomato bushy stunt virus. Plant J **33,** 949-956.

Ward, J.M., Maser, P., and Schroeder, J.I. (2009). Plant ion channels: gene families, physiology, and functional genomics analyses. Annu Rev Physiol **71,** 59-82.

Weijers, D., Sauer, M., Meurette, O., Friml, J., Ljung, K., Sandberg, G., Hooykaas, P., and Offringa, R. (2005). Maintenance of embryonic auxin distribution for apical-basal patterning by PIN-FORMED-dependent auxin transport in Arabidopsis. Plant Cell **17,** 2517-2526.

White, P.J., and Broadley, M.R. (2000). Mechanisms of ceasium uptake by plants. New Phytologist **147,** 241-256.

Wisniewska, J., Xu, J., Seifertova, D., Brewer, P.B., Ruzicka, K., Blilou, I., Rouquie, D., Benkova, E., Scheres, B., and Friml, J. (2006). Polar PIN localization directs auxin flow in plants. Science **312,** 883.

Woodward, A.W., and Bartel, B. (2005). Auxin: regulation, action, and interaction. Ann Bot **95,** 707-735.

Wu, G., Lewis, D.R., and Spalding, E.P. (2007). Mutations in Arabidopsis multidrug resistance-like ABC transporters separate the roles of acropetal and basipetal auxin transport in lateral root development. Plant Cell **19,** 1826-1837.

Yamamoto, M., and Yamamoto, K.T. (1998). Differential effects of 1-naphthaleneacetic acid, indole-3-acetic acid and 2,4-dichlorophenoxyacetic acid on the gravitropic response of roots in an auxin-resistant mutant of arabidopsis, aux1. Plant Cell Physiol **39,** 660-664.

Yang, H., and Murphy, A.S. (2009). Functional expression and characterization of Arabidopsis ABCB, AUX 1 and PIN auxin transporters in Schizosaccharomyces pombe. Plant J **59,** 179-191.

Yang, Y., Hammes, U.Z., Taylor, C.G., Schachtman, D.P., and Nielsen, E. (2006). High-affinity auxin transport by the AUX1 influx carrier protein. Curr Biol **16,** 1123-1127.

Yoo, S.D., Cho, Y.H., and Sheen, J. (2007). Arabidopsis mesophyll protoplasts: a versatile cell system for transient gene expression analysis. Nat Protoc **2,** 1565-1572.

Zhang, X.N., and Mount, S.M. (2009). Two alternatively spliced isoforms of the Arabidopsis SR45 protein have distinct roles during normal plant development. Plant Physiol **150,** 1450-1458.

Figure 1

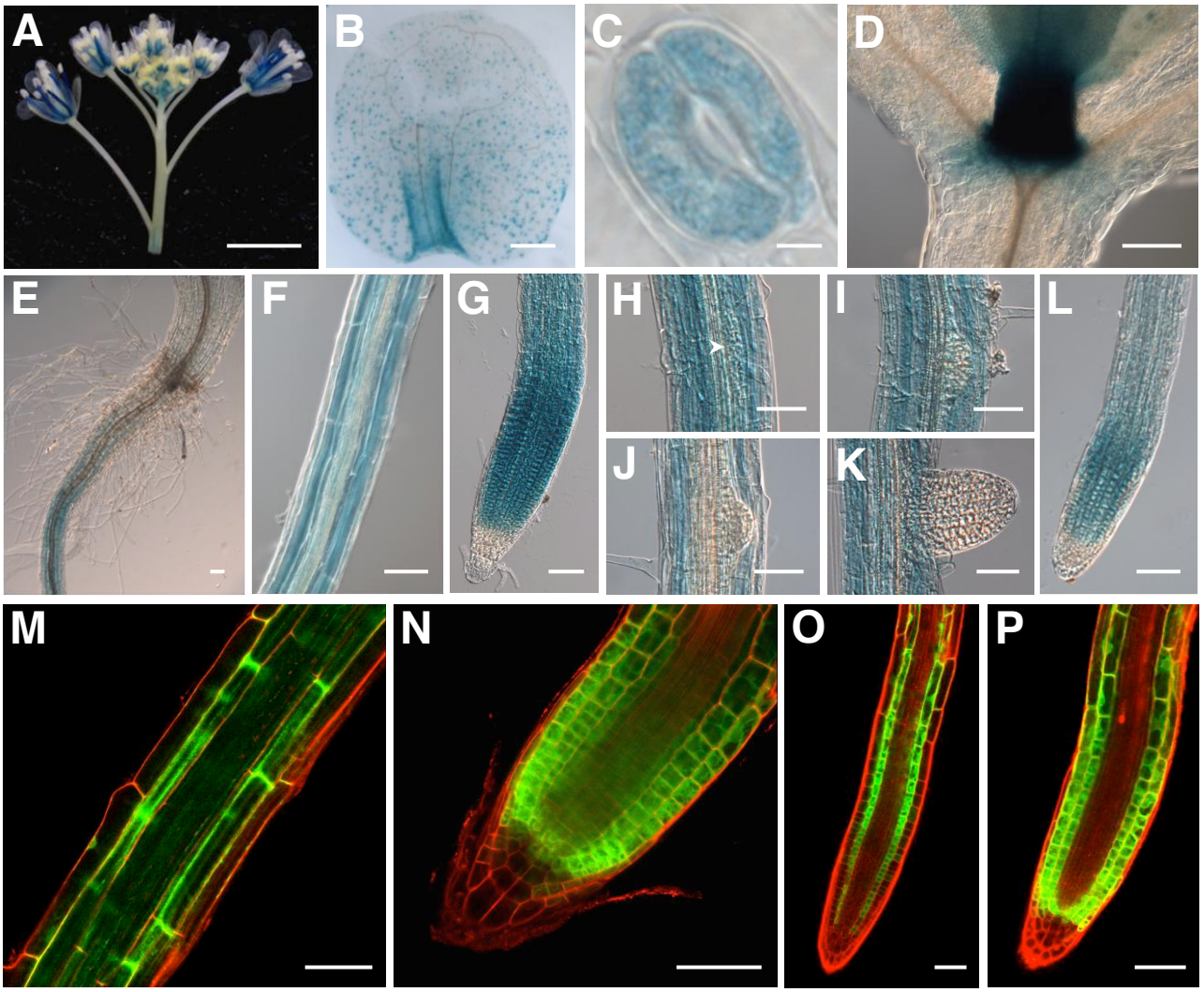

Figure 1. *ZIFL1* Promoter Activity in *Arabidopsis*.
(A) to **(L)** Differential interference contrast microscopy images of GUS-stained transgenic plants carrying the *ProZIFL1:GUS* reporter construct. *ZIFL1* promoter activity in flowers **(A)**, a young leaf **(B)**, guard cells **(C)**, the shoot apical meristem **(D)**, the hypocotyl-root junction **(E)**, the primary root **(F)**, the primary root tip **(G)**, lateral root primordia at stage II **(H)**, stage V **(I)** and stage VII **(J)**, a newly emerged lateral root **(K)** and a mature lateral root tip **(L)**. Scale bars, 1 mm (A, B), 5 µm (C) or 50 µm (D-L). The arrowhead in (H) points to new cells emanating from the pericycle.
(M) to **(P)** Confocal laser scanning microscopy images of transgenic root tissues carrying the *ProZIFL1:GFP* reporter construct. *ZIFL1* promoter activity in the primary root **(M)**, the primary root tip **(N)**, and a young **(O)** or mature **(P)** lateral root tip. Cell walls were stained with iodide propidium. The GFP and iodide propidium signals are visualized by green and red coloration, respectively. Scale bars, 50 µM.

Figure 2

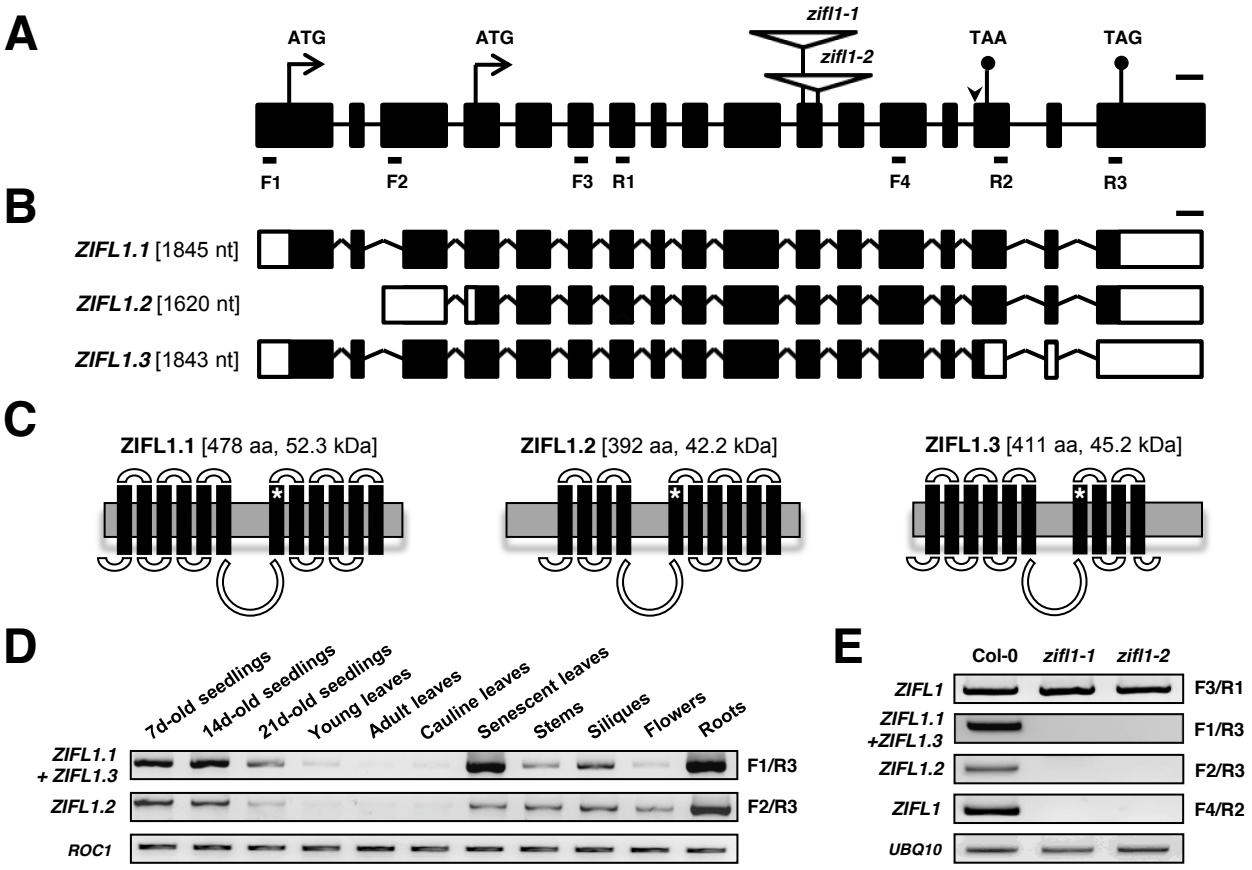

Figure 2. Structure and Expression Pattern of the ZIFL1 Isoforms.

(A) Exon/intron organization of the *ZIFL1* gene and T-DNA insertion sites in the *zifl1-1* and *zifl1-2* mutants. Boxes and lines between boxes represent exons and introns, respectively. Triangles depict the sites of the T-DNA insertions. F1, F2, F3, F4, R1, R2 and R3 indicate the location of primers used to detect *ZIFL1* expression. The arrowhead points to the alternative 3' splice site. Scale bar, 100 bp.

(B) Structure of the alternative *ZIFL1* transcripts. Boxes indicate exons with UTRs in white, and lines between boxes represent introns. Transcript lengths are indicated. Scale bar, 100 nt.

(C) Predicted topology of the three putative ZIFL1 protein isoforms. Black boxes and curved lines denote membrane-spanning segments and hydrophilic regions, respectively. Predicted isoform sizes and molecular weights are indicated. Asterisks mark the position of the predicted protein truncation in the *zifl1-1* and *zifl1-2* mutants.

(D) RT-PCR profile of *ZIFL1* expression in different plant tissues. The location of the F1, F2, and R3 primers used is shown in **(A)**. Expression of the *CYCLOPHILIN* (*ROC1*) gene was used as a loading control.

(E) RT-PCR analysis of *ZIFL1* expression in 14-d-old wild-type (Col-0) and mutant (*zifl1-1* and *zifl1-2)* seedlings. The location of the F1, F2, F3, F4, R1, R2 and R3 primers used is shown in **(A)**. Expression of the *UBIQUITIN10* (*UBQ10*) gene was used as a loading control.

Figure 3

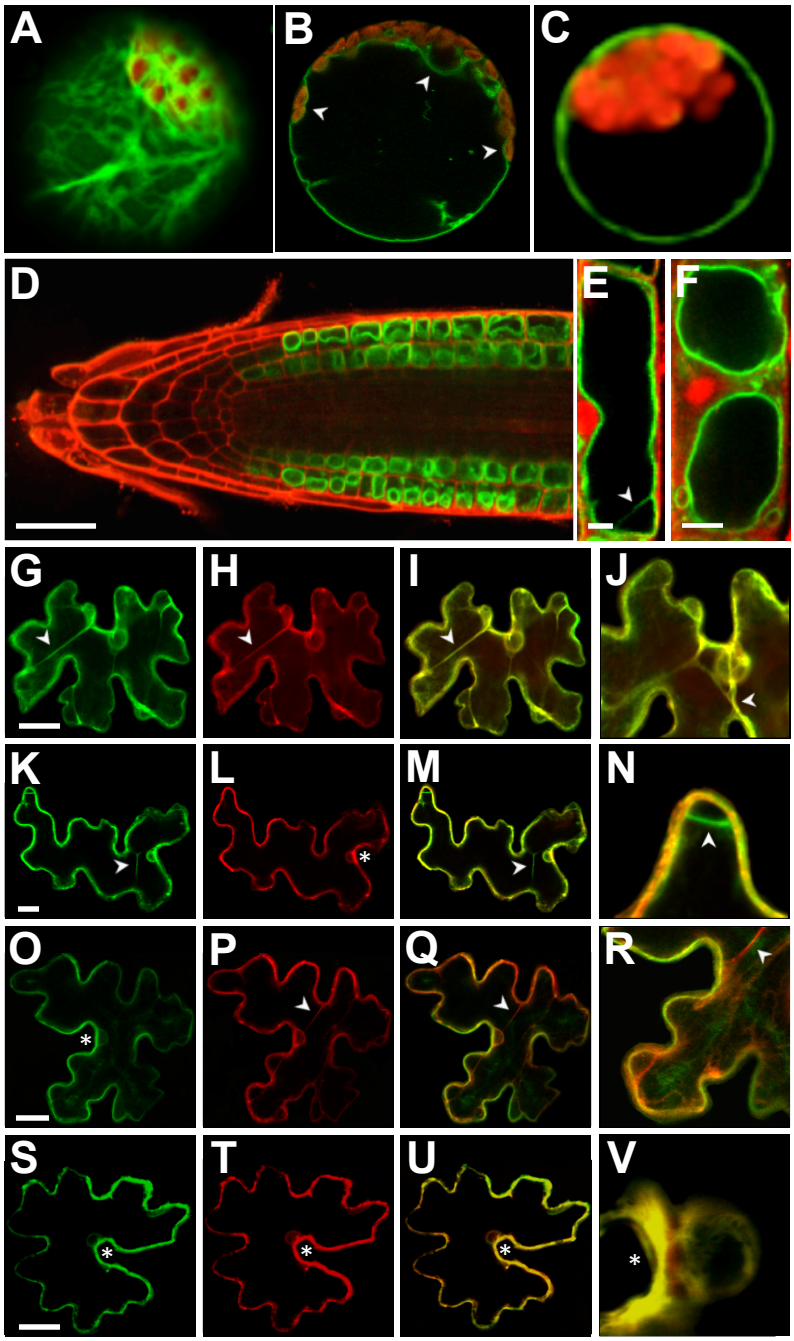

Figure 3. Subcellular Localization of the ZIFL1 Isoforms.
(A) to **(C)** Confocal laser scanning microscopy images of *Arabidopsis* wild-type mesophyll protoplasts transiently expressing either YFP alone **(A)** or the ZIFL1.1-YFP **(B)** or ZIFL1.3-YFP **(C)** fusion proteins under the control of the 35S promoter. Arrowheads point to the YFP signal on the inner side of the chloroplasts and the nucleus. The YFP and chloroplast autofluorescence signals are visualized by green and red coloration, respectively.
(D) to **(F)** Confocal laser scanning microscopy images of an *Arabidopsis zifl1-2* mutant root tip **(D)** and a mature epidermal **(E)** or cortical **(F)** root cell stably expressing the ZIFL1.1-GFP fusion protein under the control of the endogenous *ZIFL1* promoter. The GFP and iodide propidium signals are visualized by green and red coloration, respectively. The arrowhead points to a transvacuolar strand. Scale bars, 50 µm (D) and 5 µm (E, F).
(G) to **(V)** Confocal laser scanning microscopy images of tobacco leaf epidermal cells transiently co-expressing the ZIFL1.1-GFP **(G** and **K)** or the ZIFL1.3-GFP **(O** and **S)** fusion proteins with the tonoplast marker γ-TIP-mCherry **(H** and **P)** or the plasma membrane marker PIP2A-mCherry **(L** and **T)** under the control of the 35S promoter. Merged images of whole-cell (**I**, **M**, **Q** and **U**) or close-up (**J**, **N**, **R** and **V**) views are shown. Arrowheads point to transvacuolar strands and asterisks indicate fluorescence signals approaching the nucleus only on the side facing the exterior of the cell. The GFP and mCherry signals are visualized by green and red coloration, respectively. Scale bars, 20 µm.

Figure 4

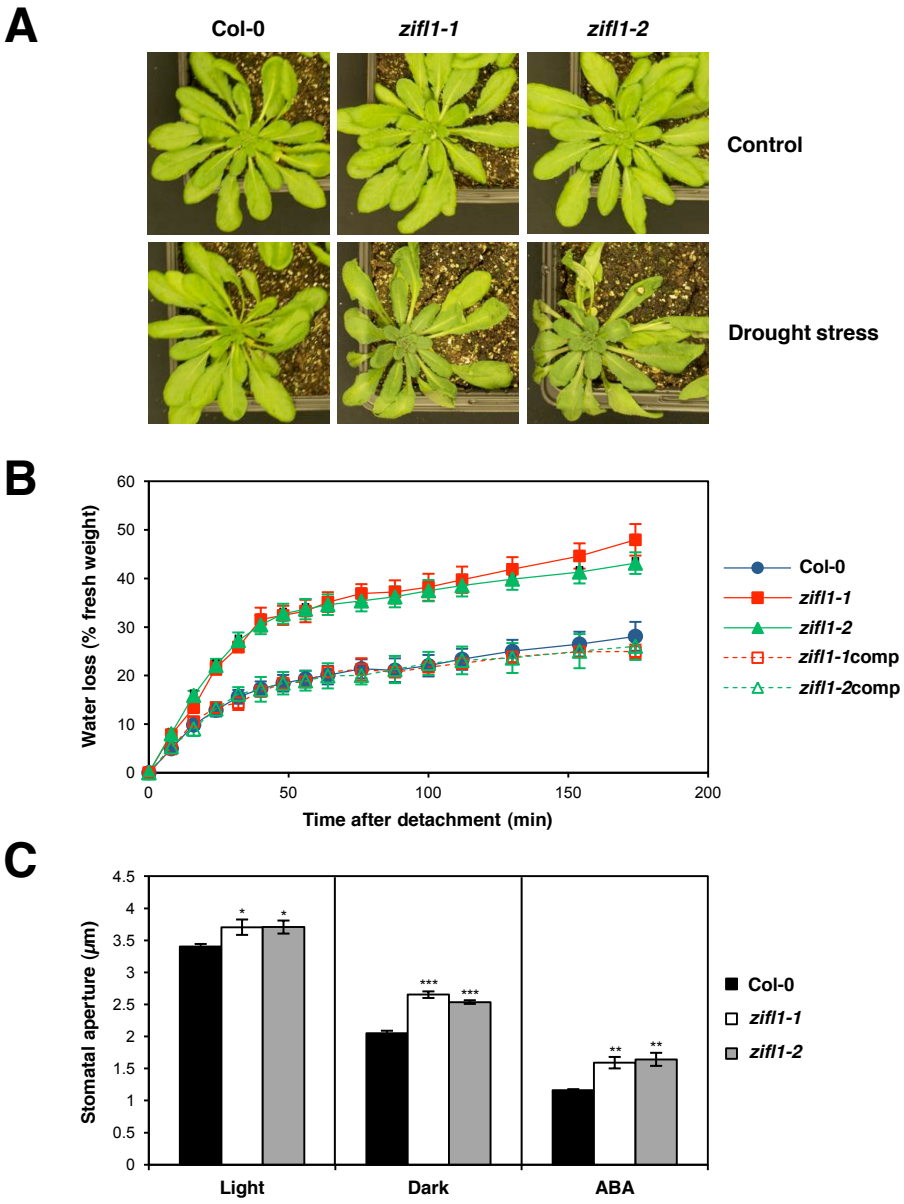

Figure 4. Drought-related Phenotypes of *ZIFL1* Loss-of-Function Mutants.
(A) Representative images of 5-week-old wild-type (Col-0) and *zifl1* mutant (*zifl1-1* and *zifl1-2*) plants grown under normal water supply (control conditions) or 7 d after terminating irrigation (drought stress).
(B) Water loss rates of rosette leaves detached from 5-week-old irrigated plants of the wild type (Col-0), the *zifl1* mutants (*zifl1-1* and *zifl1-2*) and two independent genomic complementation lines (*zifl1-1*comp and *zifl1-2*comp). Results are representative of three independent experiments and values represent means ± SD (n = 4).
(C) Stomatal apertures of rosette leaves detached from 5-week-old irrigated plants of the wild type (Col-0) and the *zifl1* mutants (*zifl1-1* and *zifl1-2*) after 3 h of light, dark or ABA (3 μM) treatment. Values represent the mean of four independent experiments ± SD. Asterisks denote statistically significant differences between *zifl1* mutants and the wild type (* P<0.05, ** P<0.01, *** P<0.001; Student's t test).

Figure 5

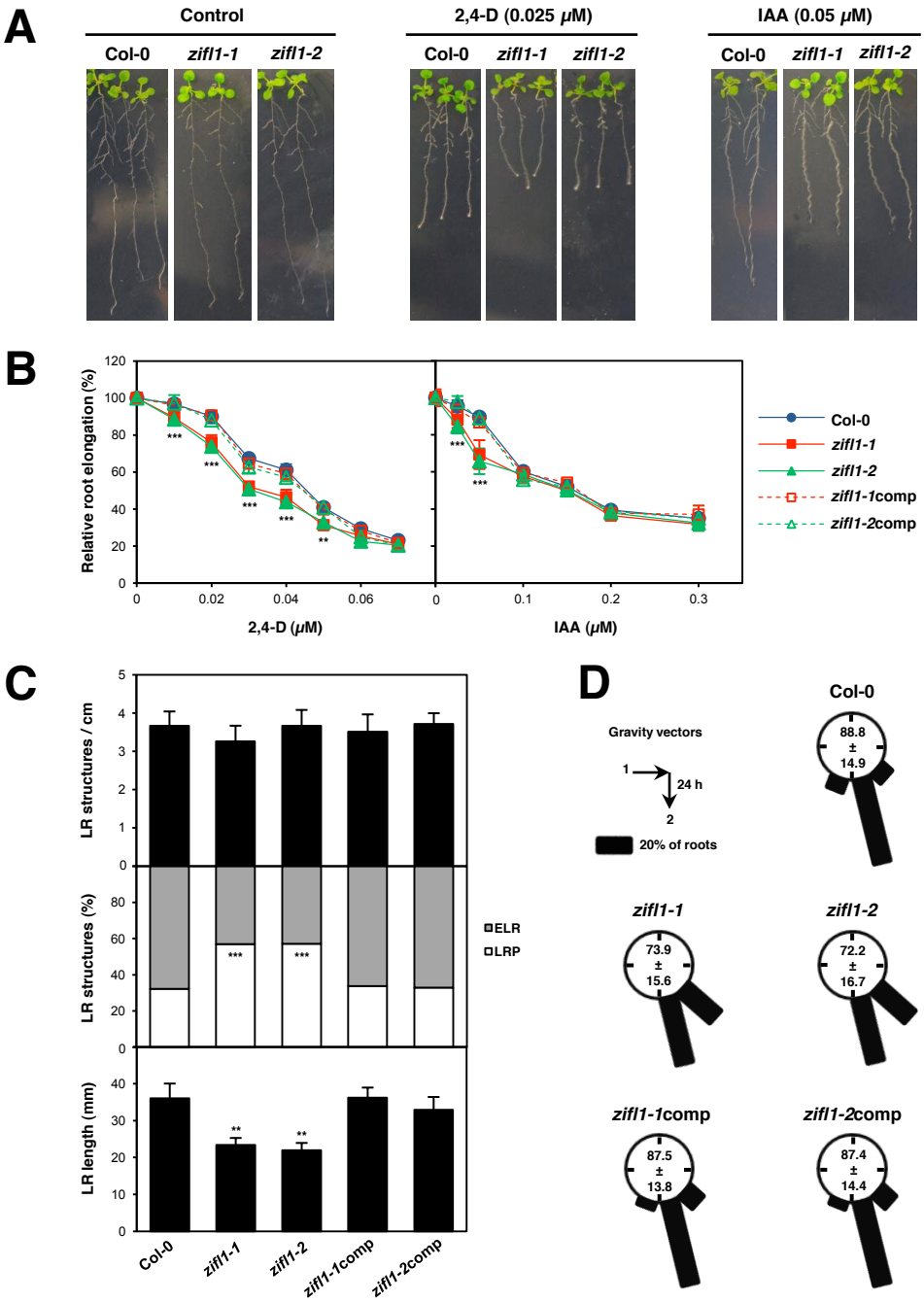

Figure 5. Auxin-related Phenotypes of *ZIFL1* Loss-of-Function Mutants.

(A) Representative images of 12-d-old wild-type (Col-0) and *zifl1* mutant (*zifl1-1* and *zifl1-2*) seedlings grown on control medium or medium supplemented with 0.025 μM 2,4-D or 0.05 μM IAA.

(B) Effect of 2,4-D (left panel) and IAA (right panel) on primary root elongation of 12-d-old seedlings of the wild type (Col-0), the *zifl1* mutants (*zifl1-1* and *zifl1-2*) and two independent genomic complementation lines (*zifl1-1*comp and *zifl1-2*comp). Results are representative of three independent experiments and values represent means ± SD (n = 16).

(C) Lateral root (LR) phenotype of 12-d-old seedlings of the wild type (Col-0), the *zifl1* mutants (*zifl1-1* and *zifl1-2*) and two independent genomic complementation lines (*zifl1-1*comp and *zifl1-2*comp). Total number of LRs (top panel), frequency of LR primordia (LRP) and emerged LRs (ELR) (middle panel) and LR length (lower panel) are presented. Results are representative of three independent experiments and bars represent means ± SD (n = 8).

(D) Root gravitropic response of 7-d-old seedlings of the wild type (Col-0), the *zifl1* mutants (*zifl1-1* and *zifl1-2*) and two independent genomic complementation lines (*zifl1-1*comp and *zifl1-2*comp) after 24 h of 90°-gravistimulation. The length of each bar represents the frequency of seedlings showing the direction of root tip curvature within the corresponding 30° sector. Results are representative of three independent experiments ($n \geq 30$).

Asterisks denote statistically significant differences between *zifl1* mutants and the wild type (** P<0.01, *** P<0.001; Student's t test).

Figure 6

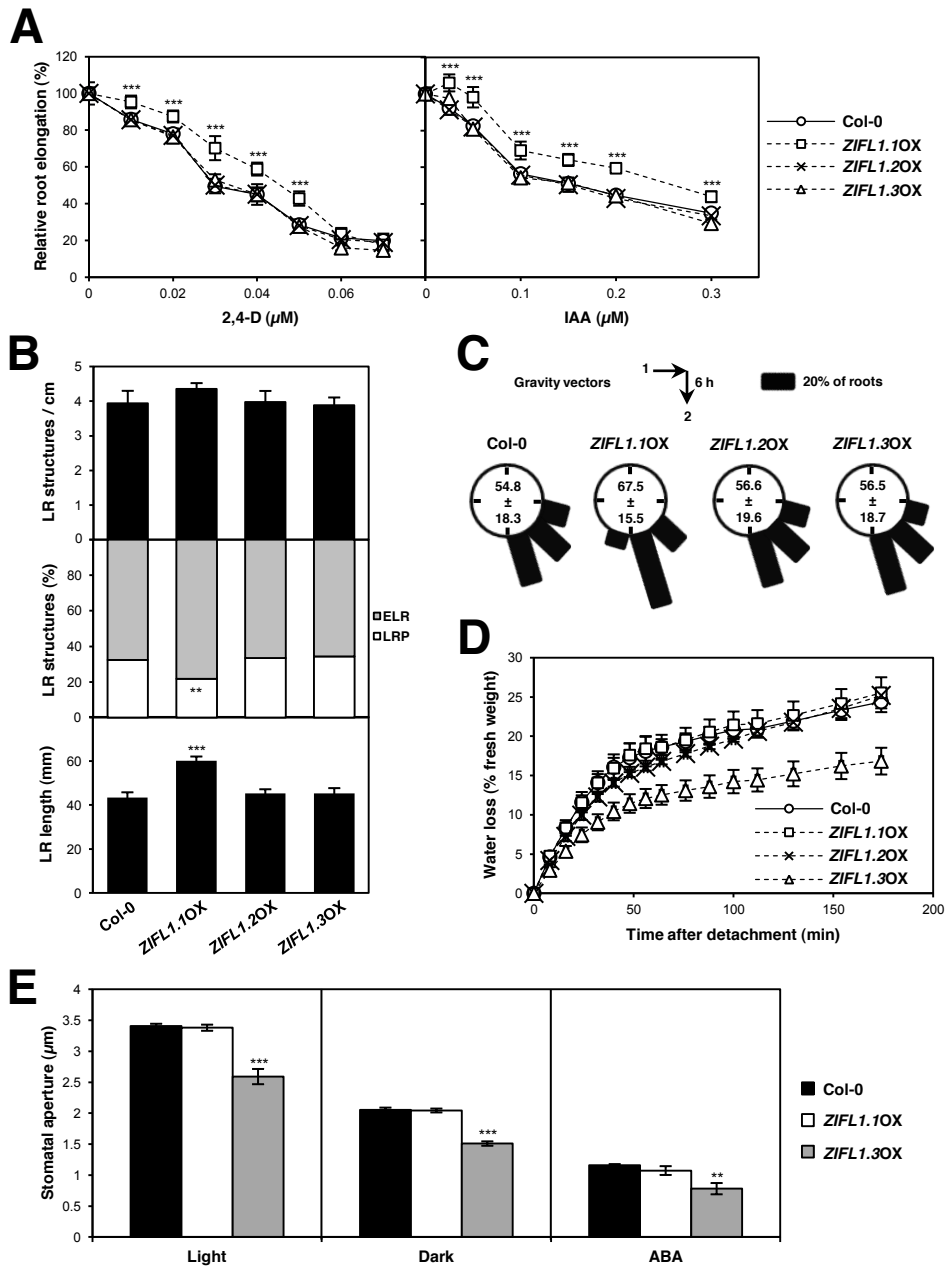

Figure 6. Phenotypes of Transgenic *Arabidopsis* Lines Overexpressing Individual ZIFL1 Isoforms.

(A) Effect of 2,4-D (left panel) and IAA (right panel) on primary root elongation of 12-d-old seedlings of the wild type (Col-0) and *ZIFL1*-overexpressing lines (*ZIFL1.1*OX, *ZIFL1.2*OX and *ZIFL1.3*OX). Results are representative of three independent experiments and values represent means ± SD (n = 16).

(B) Lateral root (LR) phenotype of 12-d-old seedlings of the wild type (Col-0) and *ZIFL1*-overexpressing lines (*ZIFL1.1*OX, *ZIFL1.2*OX and *ZIFL1.3*OX). Total number of LRs (top panel), frequency of LR primordia (LRP) and emerged LRs (ELR) (middle panel) and LR length (lower panel) are presented. Results are representative of three independent experiments and bars represent means ± SD (n = 8).

(C) Root gravitropic response of 7-d-old seedlings of the wild type (Col-0) and *ZIFL1*-overexpressing lines (*ZIFL1.1*OX, *ZIFL1.2*OX and *ZIFL1.3*OX) after 6 h of 90°-gravistimulation. The length of each bar represents the frequency of seedlings showing the direction of root tip curvature within the corresponding 30° sector. Results are representative of three independent experiments ($n \geq 30$).

(D) Water loss rates of rosette leaves detached from 5-week-old irrigated plants of the wild type (Col-0) and *ZIFL1*-overexpressing lines (*ZIFL1.1*OX, *ZIFL1.2*OX and *ZIFL1.3*OX). Results are representative of three independent experiments and values represent means ± SD (n = 4).

(E) Stomatal apertures of rosette leaves detached from 5-week-old irrigated plants of the wild type (Col-0) and *ZIFL1*-overexpressing lines (*ZIFL1.1*OX and *ZIFL1.3*OX) after 3 h of light, dark or ABA (3 μM) treatment. Values represent the mean of four independent experiments ± SD.

Asterisks denote statistically significant differences between *ZIFL1*-overexpressing lines and the wild type (** P<0.01, *** P<0.001; Student's t test).

Figure 7

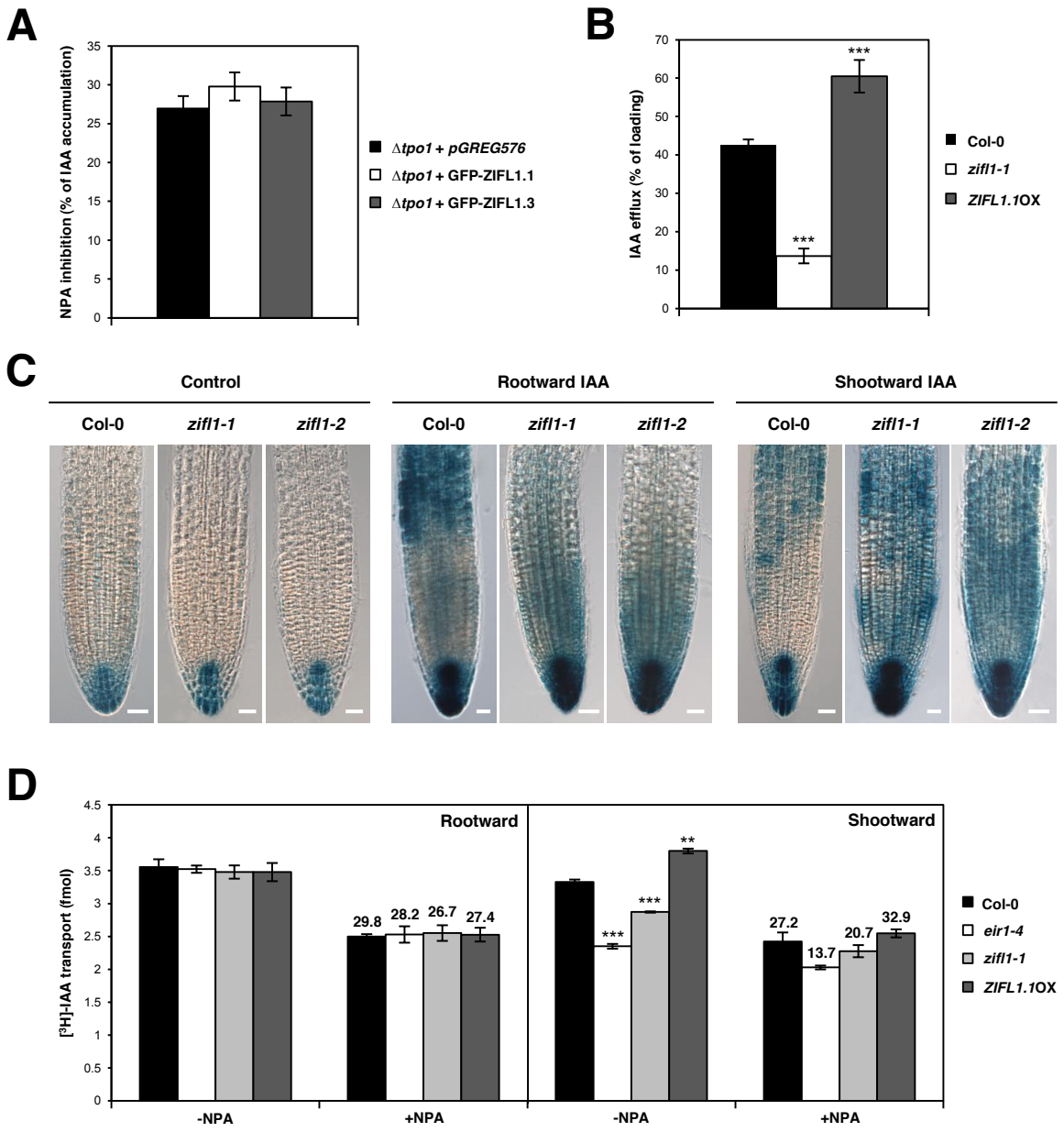

Figure 7. ZIFL1.1 IAA Transport Activity in Yeast and *Arabidopsis*.

(A) Effect of the auxin polar efflux inhibitor NPA on [^{14}C]-IAA accumulation in non-adapted yeast *Δtpo1* mutant cells harboring either the cloning vector *pGREG576* or the *pGREG576_ZIFL1.1* or *pGREG576_ZIFL1.3* plasmids. Values represent the mean of four independent experiments ± SD.

(B) IAA efflux activity of root tips from wild-type (Col-0), *zifl1-1*-mutant and *ZIFL1.1*-overexpressing (*ZIFL1.1*OX) 5-d-old seedlings. Efflux is calculated as a percentage of the initial [^{14}C]-IAA loading. Results are representative of three independent experiments and bars represent means ± SD (n = 18).

(C) Representative differential interference contrast microscopy images of primary roots from wild-type (Col-0) and *zifl1*-mutant (*zifl1-1* and *zifl1-2*) 5-d-old seedlings expressing the auxin-responsive Pro*DR5:GUS* construct. Seedlings were either not treated (Control) or treated with 1 µM IAA for 3 h at the hypocotyl-root junction (Rootward IAA) or at the root tip (Shootward IAA). Scale bars, 25 µm.

(D) Rootward and shootward IAA transport in primary roots from 5-d-old seedlings of the wild type (Col-0), the *eir1-4* and *zifl1-1* mutants, and the *ZIFL1.1*OX transgenic line in the absence (-NPA) or presence (+NPA) of 10 µM NPA. Values represent the mean of three independent experiments ± SD. For each genotype, the percentage of root IAA transport inhibition by NPA is indicated above the corresponding bars (P<0.01 for all genotypes in both polarities, except for shootward transport in *ZIFL1.1*OX where P<0.001).

Asterisks denote statistically significant differences between *zifl1* mutants or the *ZIFL1.1*OX line and the wild type (** P<0.01, *** P<0.001; Student's t test).

Figure 8

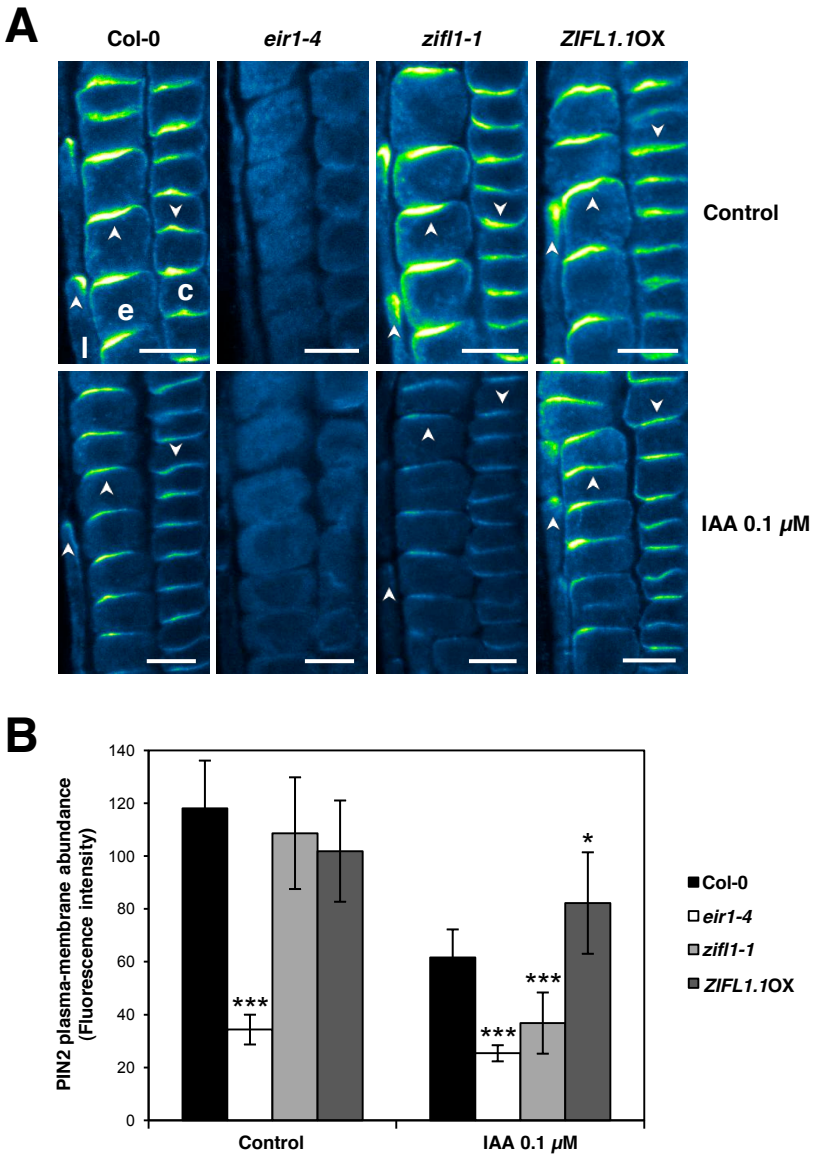

Figure 8. PIN2 Immunolocalization in *Arabidopsis zifl1-1* Mutant and *ZIFL1.1*-overexpressing Root Tips.

(A) Representative confocal laser scanning microscopy images of the PIN2 signal in root tips from 5-d-old wild-type (Col-0), *eir1-4* and *zifl1-1* mutant, and *ZIFL1.1*-overexpressing seedlings treated or not for 2 d with 0.1 μM IAA. Detection settings for staining visualization were identical for all genotypes. Arrowheads indicate the polarity of PIN2 localization. l, lateral root cap; c, cortex; e, epidermis. Signal intensities are coded blue to yellow corresponding to increasing intensity levels. Scale bars, 10 μm.

(B) Quantification of the PIN2 signal at the plasma membrane in root tip epidermal cells from seedlings of the wild type (Col-0), the *eir1-4* and *zifl1-1* mutants, and the *ZIFL1.1*OX transgenic line. Average fluorescence (pixel) intensity values represent the mean of three independent experiments ± SD (n > 24). Asterisks denote statistically significant differences from the wild type under each condition (* P<0.05, *** P<0.001; Student's t test).

Figure 9

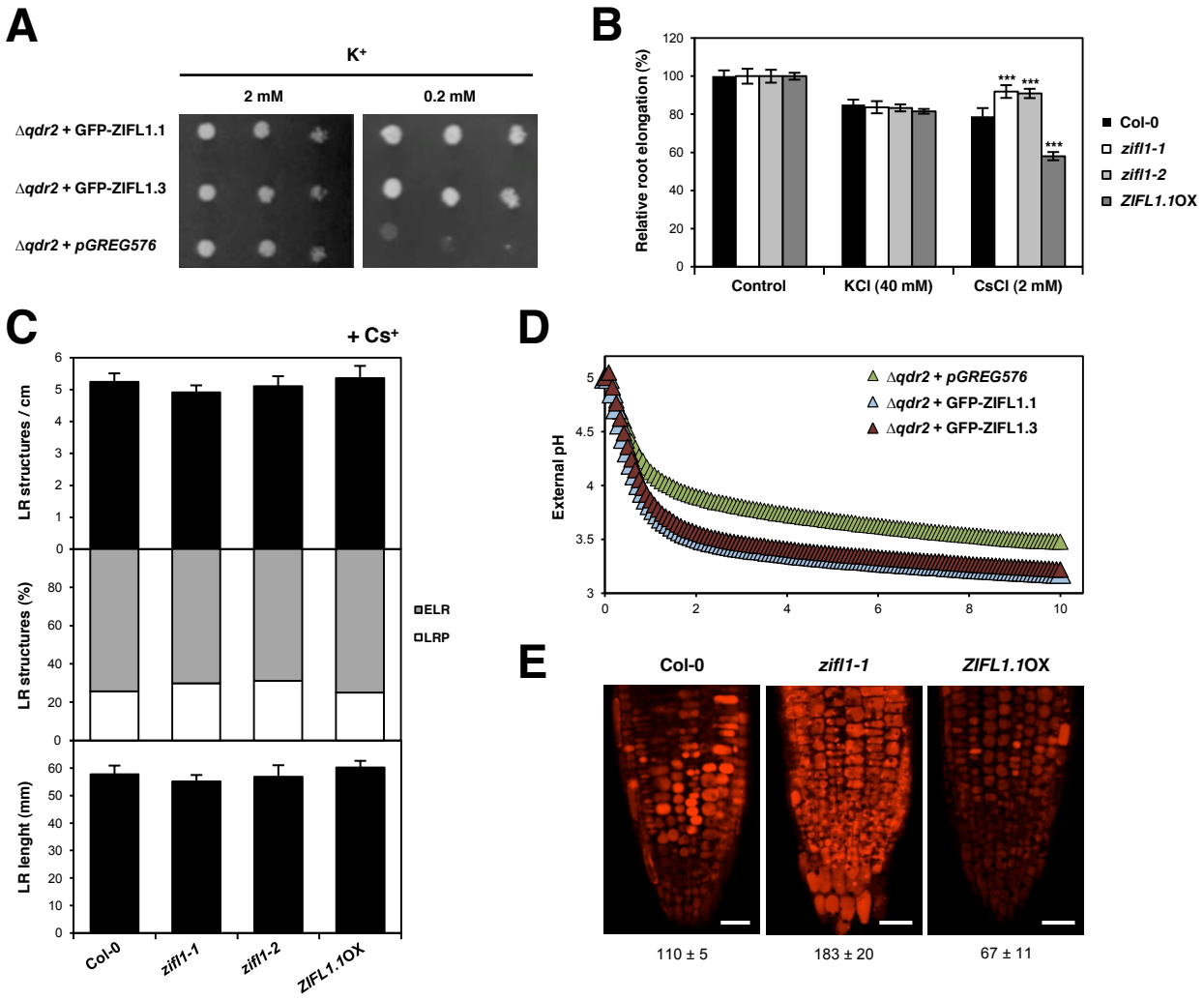

Figure 9. Potassium and Proton Transport Activity of ZIFL1.1 and ZIFL1.3 in Yeast and *Arabidopsis*.
(A) Susceptibility to low potassium growth conditions of yeast *Δqdr2* mutant cells harboring either the cloning vector *pGREG576* or the *pGREG576_ZIFL1.1* or *pGREG576_ZIFL1.3* plasmids determined by spotting dilution series of cell suspensions (1, 1:5, and 1:10).
(B) Effect of K^+ and Cs^+ on primary root elongation of 12-d-old seedlings of the wild type (Col-0), the *zifl1* mutants (*zifl1-1* and *zifl1-2*) and the *ZIFL1.1*OX transgenic line. Results are representative of three independent experiments and bars represent means ± SD (n = 16). Asterisks denote statistically significant differences between *zifl1* mutants or the *ZIFL1.1*OX line and the wild type (*** P<0.001; Student's t test).
(C) Lateral root (LR) phenotype of 12-d-old seedlings of the wild type (Col-0), the *zifl1* mutants (*zifl1-1* and *zifl1-2*) and the *ZIFL1.1*OX line in the presence of 2 mM Cs^+. Total number of LRs (top panel), frequency of LR primordia (LRP) and emerged LRs (ELR) (middle panel) and LR length (lower panel) are presented. Results are representative of three independent experiments and bars represent means ± SD (n = 8).
(D) External medium acidification promoted by energized yeast *Δqdr2* mutant cells harboring either the cloning vector *pGREG576* or the *pGREG576_ZIFL1.1* or *pGREG576_ZIFL1.3* plasmids. Results are representative of three independent experiments.
(E) Confocal laser scanning microscopy images of *Arabidopsis* root tip epidermal cells of 5-d-old wild-type, *zifl1-1*-mutant and *ZIFL1.1*-overexpressing seedlings stained with acridine orange. Detection settings for staining visualization were identical for all genotypes, and numbers below each image indicate the average fluorescence (pixel) intensity representative of one of three independent experiments (means ± SD, n = 8). Scale bars, 25 μm.

Figure S1

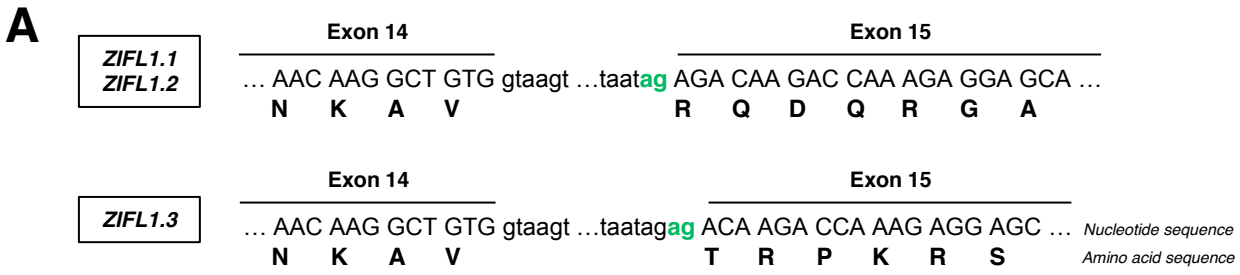

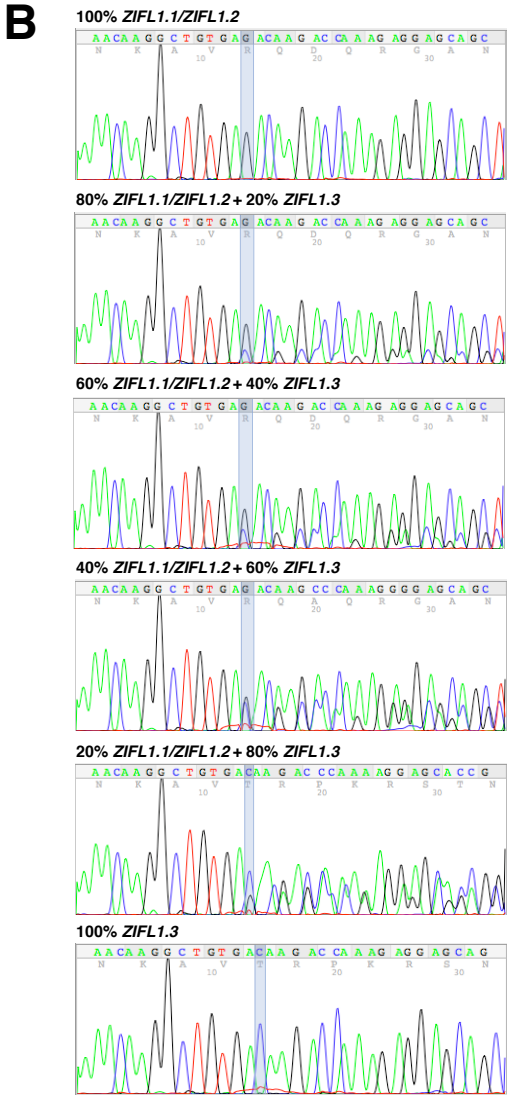

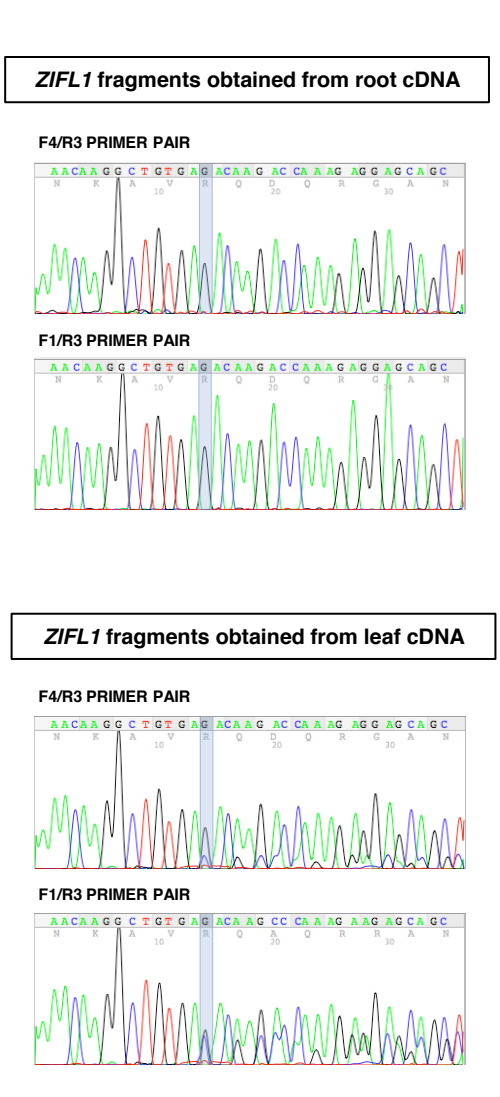

Figure S1. Sequencing Analysis of the *ZIFL1* Transcript Tissue Distribution.
(A) Schematic representation of the alternative 3' splice site selection event in intron 14 of the *ZIFL1* pre-mRNA. The nucleotide sequence of the *ZIFL1.1*/*ZIFL1.2* (top) and *ZIFL1.3* (bottom) transcripts is shown, along with the amino acid sequence of the encoded proteins. Exon and intron sequences are shown in upper and lower case, respectively. For each transcript, the green letters indicate which of the two consecutive AGs is selected at the 3' splice site.
(B) Control chromatograms obtained upon sequencing of PCR products amplified from cloned *ZIFL1.1/ZIFL1.2* or *ZIFL1.3* fragments. The proportion of each product included in the sequence reaction is indicated.
(C) Representative chromatograms obtained upon sequencing of PCR products amplified from root- or leaf-derived cDNA. The location of the primer pairs used (F4/R3, which amplifies all three *ZIFL1* transcripts, and F1/R3, detecting exclusively *ZIFL1.1* and *ZIFL1.3*) is shown in Figure 2A. Identical results were obtained after analysis of four independent samples for each tissue.

Figure S2

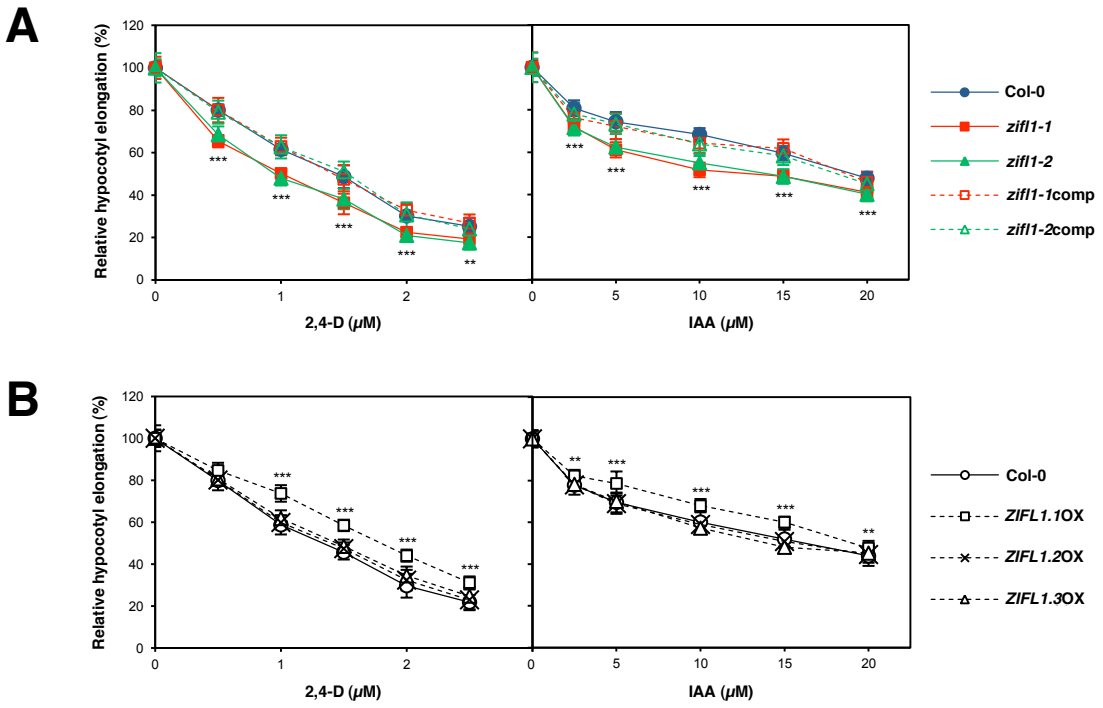

Figure S2. Auxin-related Hypocotyl Phenotype of *ZIFL1* Loss-of-Function Mutants and *ZIFL1*-overexpressing Lines.

(A) Effect of 2,4-D (left panel) and IAA (right panel) on hypocotyl elongation of 7-d-old dark-grown seedlings of the wild type (Col-0), the *zifl1* mutants (*zifl1-1* and *zifl1-2*) and two independent genomic complementation lines (*zifl1-1*comp and *zifl1-2*comp). Results are representative of three independent experiments and values represent means ± SD (*n* = 40-60).

(B) Effect of 2,4-D (left panel) and IAA (right panel) on hypocotyl elongation of 7-d-old dark-grown seedlings of the wild type (Col-0) and *ZIFL1*-overexpressing lines (*ZIFL1.1*OX, *ZIFL1.2*OX and *ZIFL1.3*OX). Results are representative of three independent experiments and values represent means ± SD (*n* = 40-60).

Figure S3

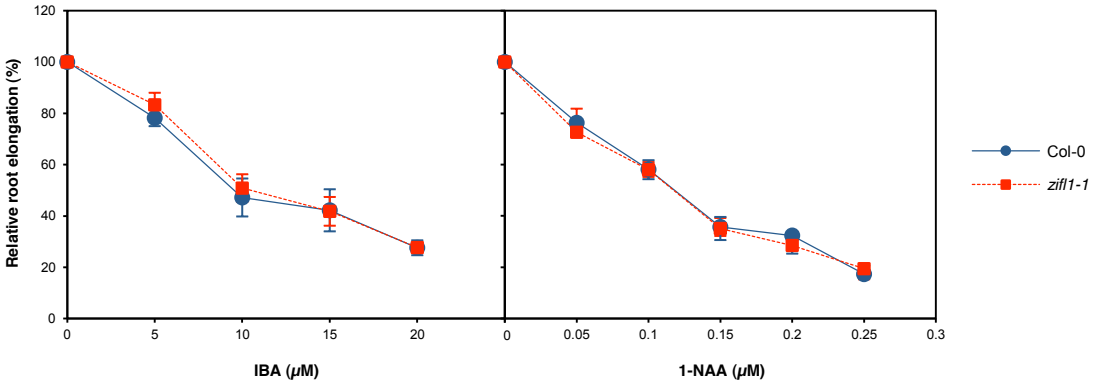

Figure S3. Effect of IBA and 1-NAA on the *zifl1-1* Mutant.
Effect of IBA (left panel) and 1-NAA (right panel) on primary root elongation of 12-d-old seedlings of the wild type (Col-0) and the *zifl1-1* mutant. Results are representative of two independent experiments and values represent means ± SD (*n* = 16).

Figure S4

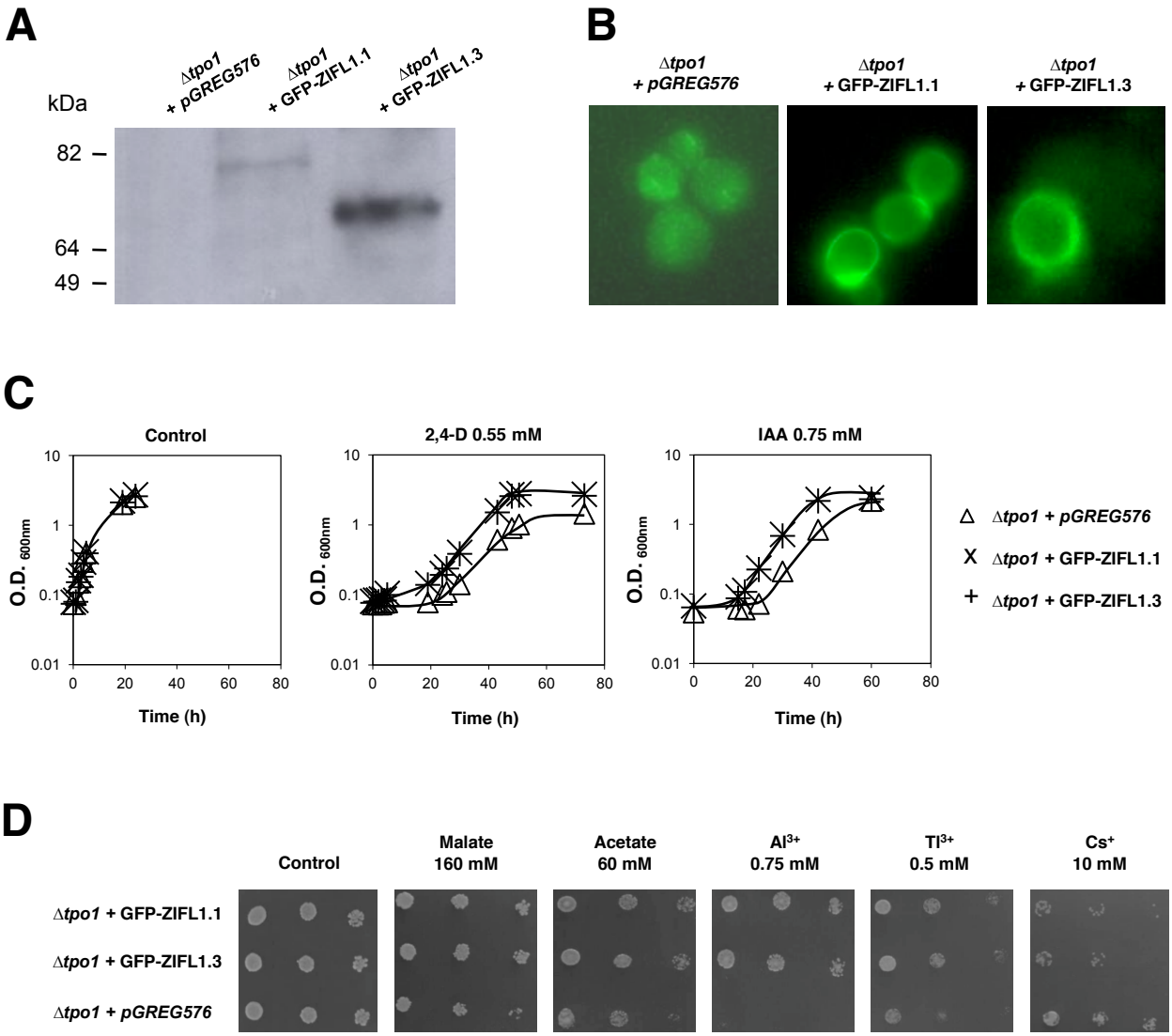

Figure S4. Heterologous Expression of ZIFL1.1 and ZIFL1.3 in Yeast.

(A) Western blot analysis of GFP-ZIFL1.1 and GFP-ZIFL1.3 fusion proteins in yeast *Δtpo1* mutant cells using anti-GFP antibodies.

(B) Fluorescence microscopy images of exponential-phase yeast *Δtpo1* mutant cells harboring either the cloning vector *pGREG576* or the *pGREG576_ZIFL1.1* or *pGREG576_ZIFL1*.3 plasmids after induction of recombinant protein production.

(C) Comparison of the growth curves of non-adaptated yeast *Δtpo1* mutant cells in liquid medium unsupplemented or supplemented with 2,4-D or IAA, harboring either the cloning vector *pGREG576* or the *pGREG576_ZIFL1.1* or *pGREG576_ZIFL1.3* plasmids. Results are representative of three independent experiments.

(D) Susceptibility to malate, acetate, Al^{3+}, Tl^{3+} and C^{s+} of yeast *Δtpo1* mutant cells harboring either the cloning vector *pGREG576* or the *pGREG576_ZIFL1.1* or pGREG576_*ZIFL1*.3 plasmids by spotting dilution series of cell suspensions (1, 1:5, and 1:10).

Figure S5

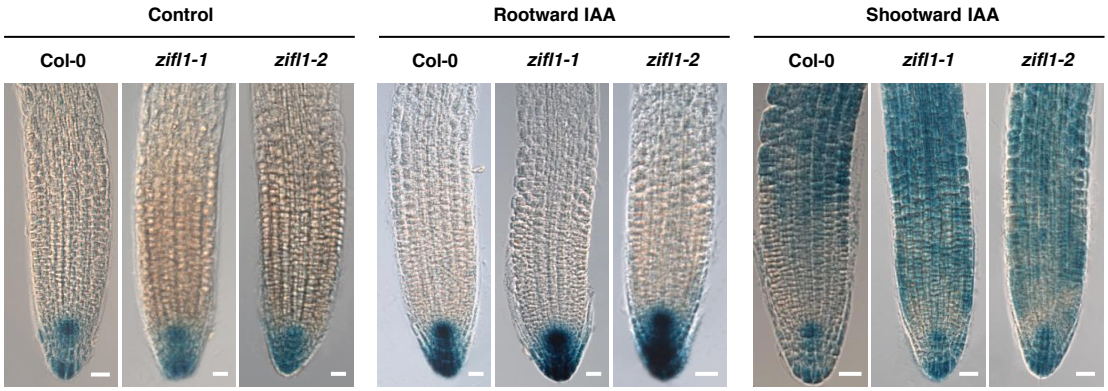

Figure S5. Auxin-responsive Pro*DR5:GUS* Expression in Wild-type and *zifl1* Mutant Roots.
Representative differential interference contrast microscopy images of primary roots from wild-type (Col-0) and *zifl1*-mutant (*zifl1-1* and *zifl1-2*) 5-d-old seedlings expressing the auxin-responsive Pro*DR5:GUS* construct. Seedlings were either not treated (Control) or treated with 0.5 µM IAA for 3 h at the hypocotyl-root junction (Rootward IAA) or at the root tip (Shootward IAA). Scale bars, 25 µm.

Table S1. Benzoic Acid (BA) Diffusion in Roots of the Wild Type, *eir1-4* and *zifl1-1* Mutants and *ZIFL1.1*-overexpressing Lines.

	BA diffusion (fmol)			
	Rootward		Shootward	
	-NPA	+NPA	-NPA	+NPA
Col-0	0.43 ± 0.05	0.31 ± 0.13	0.55 ± 0.16	0.49 ± 0.14
eir1-4	0.48 ± 0.14 (0.41)	0.32 ± 0.15 (0.48)	0.49 ± 0.08 (0.41)	0.50 ± 0.18 (0.48)
zifl1-1	0.44 ± 0.09 (0.46)	0.36 ± 0.16 (0.37)	0.73 ± 0.21 (0.20)	0.58 ± 0.18 (0.30)
*ZIFL1.1*OX	0.40 ± 0.12 (0.45)	0.49 ± 0.10 (0.10)	0.72 ± 0.12 (0.15)	0.52 ± 0.17 (0.43)

Results are representative of two independent experiments and values represent means ± SD (n = 10).
Numbers between parentheses indicate the P values (wild type versus *eir1-4* or *zifl1-1* mutants or *ZIFL1*OX line) obtained by Student's t test.

Table S2. Sequences of Used Primers.

PRIMER NAME	SEQUENCE
Expression analyses	
F1	5'-GAGAGTACGTGAAAACC-3'
F2	5'-CTTCTGTTACGTGGTGATT-3'
F3	5'-ATTCCCCTTTCTCTACTTTA-3'
F4	5'-TTTAGCCCTTACCGTGACT-3'
R1	5'-GCCAATGATGAGTCCA-3'
R2	5'-CATTAGCTGCTCCTCTTTGG-3'
R3	5'-CTGTTGTGTTTCAGCTA-3'
ROC1F	5'-GTCTGATAGAGATCTCACGT-3'
ROC1R	5'-AATCGGCAACAACAACAGGC-3'
UBQ10F	5'-GATCTTTGCCGGAAAACAATTGG-3'
UBQ10R	5'-TAGAAAGAAAGAGATAACAGG-3'
Cloning of Pro*ZIFL1*:*GUS-GFP* construct	
ProZIFL1F	5'-TT*GAGCTC*TCAGATACGAAAGAAACCG-3'
ProZIFL1R	5'-TT*CCGCGG*TTCCACACACCTCTCTAATC-3'
Cloning of Pro*ZIFL1*:*ZIFL1* construct	
ZIFL1compF	5'-TT*AAGCTT*TCAGATACGAAAGAAACCG-3'
ZIFL1compR	5'- TT*TCTAGA*CTGTTGCACCCATTGA-3'
Cloning of Pro*35S*:*ZIFL1-YFP* and Pro*ZIFL1*:*ZIFL1-G*FP constructs	
ZIFL1.1-YFPF	5'-TT*CTCGAG*GAGAGTACGTGAAAACC-3'
ZIFL1.1-YFPR	5'-TT*AATTAA*CTGTTGTGTTTCAGCTA-3'
ZIFL1.2-YFPF	5'-TT*CTCGAG*CTTCTGTTACGTGGTGATT-3'
ZIFL1.2-YFPR	5'-TT*TTAATTAA*CTGTTGTGTTTCAGCTA-3'
ZIFL1.3-YFPF	5'-TT*CTCGAG*GAGAGTACGTGAAAACC-3'
ZIFL1.3-YFPR	5'-TT*TTAATTAA*GCTGCTCCTCTTTGGTCTTGTCA-3'
Cloning of Pro*35S*:*ZIFL1* constructs	
ZIFL1.1-OEF	5'-TT*CTCGAG*GAGAGTACGTGAAAACC-3'
ZIFL1.1-OER	5'-TT*GGCGCGCC*CTGTTGTGTTTCAGCTA-3'
ZIFL1.2-OEF	5'-TT*CTCGAG*CTTCTGTTACGTGGTGATT-3'
ZIFL1.2-OER	5'-TT*GGCGCGCC*CTGTTGTGTTTCAGCTA-3'
ZIFL1.3-OEF	5'-TT*CTCGAG*GAGAGTACGTGAAAACC-3'
ZIFL1.3-OER	5'-TT*GGCGCGCC*GCTGCTCCTCTTTGGTCTTGTCA-3'

Restriction sites are shown in italics and underlined.